Influence of Wind Tunnel Noise on the Location of Boundary-Layer Transition on a Slender Cone at Mach Numbers from 0.2 to 5.5

Volume I
Experimental Methods and Summary of Results

N. Sam Dougherty, Jr.
ARO, Inc.

March 1980

Final Report for Period January 26, 1970 – April 28, 1977

Approved for public release; distribution unlimited.

ARNOLD ENGINEERING DEVELOPMENT CENTER
ARNOLD AIR FORCE STATION, TENNESSEE
AIR FORCE SYSTEMS COMMAND
UNITED STATES AIR FORCE

NOTICES
When U. S. Government drawings, specifications, or other data are used for any purpose other than a definitely related Government procurement operation, the Government thereby incurs no responsibility nor any obligation whatsoever, and the fact that the Government may have formulated, furnished, or in any way supplied the said drawings, specifications, or other data, is not to be regarded by implication or otherwise, or in any manner licensing the holder or any other person or corporation, or conveying any rights or permission to manufacture, use, or sell any patented invention that may in any way be related thereto.
Qualified users may obtain copies of this report from the Defense Technical Information Center.
References to named commerical products in this report are not to be considered in any sense as an indorsement of the product by the United States Air Force or the Government.

This report has been reviewed by the Office of Public Affairs (PA) and is releasable to the National Technical Information Service (NTIS). At NTIS, it will be available to the general public, including foreign nations.

APPROVAL STATEMENT

This report has been reviewed and approved.

Alexander F. Money

ALEXANDER F. MONEY
Project Manager
Directorate of Technology

Approved for publication:

FOR THE COMMANDER

Marion L. Laster

MARION L. LASTER
Director of Technology
Deputy for Operations

REPORT DOCUMENTATION PAGE		READ INSTRUCTIONS BEFORE COMPLETING FORM
1. REPORT NUMBER AEDC-TR-78-44	2. GOVT ACCESSION NO.	3. RECIPIENT'S CATALOG NUMBER
4. TITLE *(and Subtitle)* INFLUENCE OF WIND TUNNEL NOISE ON THE LOCATION OF BOUNDARY-LAYER TRANSITION ON A SLENDER CONE AT MACH NUMBERS FROM 0.2 TO 5.5 Volume I: Experimental Methods and Summary of Results		5. TYPE OF REPORT & PERIOD COVERED Final Report-January 26, 1970-April 28, 1977 6. PERFORMING ORG. REPORT NUMBER
7. AUTHOR*(s)* N. Sam Dougherty, Jr., ARO, Inc. a Sverdrup Corporation Company		8. CONTRACT OR GRANT NUMBER*(s)*
9. PERFORMING ORGANIZATION NAME AND ADDRESS Arnold Engineering Development Center/DOT Air Force Systems Command Arnold Air Force Station, Tennessee 37389		10. PROGRAM ELEMENT, PROJECT, TASK AREA & WORK UNIT NUMBERS Program Element 65807F
11. CONTROLLING OFFICE NAME AND ADDRESS Arnold Engineering Development Center/DOS Air Force Systems Command Arnold Air Force Station, Tennessee 37389		12. REPORT DATE March 1980 13. NUMBER OF PAGES 49
14. MONITORING AGENCY NAME & ADDRESS*(if different from Controlling Office)*		15. SECURITY CLASS. *(of this report)* UNCLASSIFIED 15a. DECLASSIFICATION DOWNGRADING SCHEDULE N/A

16. DISTRIBUTION STATEMENT *(of this Report)*

Approved for public release; distribution unlimited.

17. DISTRIBUTION STATEMENT *(of the abstract entered in Block 20, if different from Report)*

18. SUPPLEMENTARY NOTES

Available in Defense Technical Information Center (DTIC).

19. KEY WORDS *(Continue on reverse side if necessary and identify by block number)*

wind tunnels	slender bodies	transonic flow
noise	Mach numbers	supersonic flow
boundary-layer transition	Reynolds numbers	
conical bodies	subsonic flow	

20. ABSTRACT *(Continue on reverse side if necessary and identify by block number)*

A study was conducted to investigate the effects of wind tunnel noise on the location of boundary-layer transition. The study was carried out by conducting experiments on a particular slender, highly polished cone having an included angle of 10 deg. Wind tunnel noise levels were measured in the test section by flush-mounted microphones imbedded in the cone surface. The measurement of boundary-layer transition location was made using

DD FORM 1 JAN 73 1473 EDITION OF 1 NOV 65 IS OBSOLETE

20. ABSTRACT (Continued)

either a traversing pitot pressure probe in contact with the cone surface or the flush-mounted microphones. The experiments were carried out in 23 different subsonic, transonic, and supersonic wind tunnels over a range of Mach numbers from 0.2 to 5.5 and a unit Reynolds number range from 1.0×10^6 to 7.0×10^6 per foot, the bulk of the data being obtained for a range from 2.0×10^6 to 4.0×10^6 per foot. The results clearly show a strong influence of wind tunnel noise on boundary-layer transition location correlatable with overall root-mean-square noise levels. Because the noise level generally varied with Mach number and unit Reynolds number, the unit Reynolds number was found to have little effect on transition Reynolds number.

AFSC
Arnold AFS Tenn

PREFACE

The research reported herein was conducted by the Arnold Engineering Development Center (AEDC), Air Force Systems Command (AFSC), under Program Element 65807F. The Air Force project manager was A. F. Money. The results were obtained by ARO, Inc., AEDC Division (a Sverdrup Corporation Company), operating contractor for the AEDC, AFSC, Arnold Air Force Station, Tennessee, under ARO Project Nos. PW5201, PW5301, PF206, PF406, P32A-B0A, and P32A-G2A. Data presented in this report were acquired in cooperation with the NASA/Langley Aeronautical Research Center and Ames Research Center, the Naval Ship Research and Development Center, the Calspan Corporation, and three Western European governments: the United Kingdom, France, and the Netherlands. The manuscript was submitted for publication on June 26, 1978.

The author wishes to acknowledge contributions to this work from several persons within Sverdrup/ARO, Inc.: Dr. M. D. High, O. P. Credle, H. T. Jones, R. G. Butler, R. E. Rieben, J. A. Benek, and J. S. Hahn. The author wishes to acknowledge the special contributions of Capt. Carlos Tirres, USAF, as project monitor for AEDC during most of this work. Furthermore, the author wishes to acknowledge the efforts of several persons outside AEDC in the acquisition of data from many facilities, in particular: F. W. Steinle, Jr., NASA/ Ames Research Center; R. L. Stallings, Jr. and J. T. Foughner, NASA/Langley Research Center; D. G. Mabey, U.K. Royal Aircraft Establishment; X. Vaucheret, Office National D'Etudes et de Recherches Aerospatiales; Dr. R. Ross, National Luchten Ruimtevaartlaboratorium (NLR); R. Jordan, Aeronautical Research Association, Ltd., U.K.; D. Davidson, Naval Ship Research and Development Center; R. de Kuyper, Calspan Corporation; and Col. D. H. Daley, USAF, while at the USAF European Office of Aerospace Research.

CONTENTS

ILLUSTRATIONS

TABLES

INTRODUCTION

The correlation of the point of laminar boundary-layer transition on a body tested in the aerodynamic and turbulent environment of a wind tunnel to that which would occur on the same body in free flight has been a long-sought and elusive goal. The motivation for obtaining such a correlation is the refinement of extrapolations of Reynolds-number-sensitive data from aerodynamic tests in wind tunnels to the flight envelope of full-scale vehicles.

In cases of natural transition, one cannot expect a constancy to exist in transition Reynolds numbers relative to characteristic length Reynolds numbers. This fact was recognized early at the Arnold Engineering Development Center (AEDC) and led to the proposal by Potter and Whitfield, Refs. 1 and 2, that the unit Reynolds number was a significant parameter in laminar boundary-layer stability. Because of the significance of laminar-to-turbulent transition on all of the subsequent events that can happen in the boundary layer on a body, transition Reynolds number is an extremely important parameter in Reynolds number scaling. Because laminar-to-turbulent transition is influenced by free-stream disturbances in wind tunnels, imprecise knowledge of the behavior of transition under the action of free-stream disturbances is a factor in the degree of inaccuracy in the simulation afforded by wind tunnels.

Experimental research on transition at AEDC has been primarily macroscopic, focused on effects of geometry, controlled roughness, and facility environmental influence as they are related to the problem of simulation. Following a decade of supersonic and hypersonic measurements such as reported by Potter and Whitfield (e.g., Refs. 3, 4, and 5), Pate and Schueler were able to demonstrate the existence of a definable facility environmental influence in some ten different facilities at Mach numbers from 3.0 to 8.0 on conical and planar transition (Refs. 6 and 7). The present research is an extension of the earlier work in transition, to lower Mach numbers, focusing on the influence of the transonic and low supersonic wind tunnel test section flow environment.

A sharp, slender cone was chosen for the experimental model. Transition data were acquired in subsonic, transonic, and supersonic wind tunnels following the prior high-speed experience with cones, e.g., Ref. 7. This cone was instrumented with microphones to allow for some degree of measurement of tunnel test section free-stream acoustic levels, the microphones being flush-mounted on the cone surface similarly to those used in supersonic boundary-layer studies by Pate and Brown, Ref. 8. Early results using this cone in several transonic wind tunnels were reported by Credle and Carleton in Ref. 9 (two tunnels) and by Dougherty and Steinle in Ref. 10 (six tunnels). The tunnels in which the cone was tested included facilities of the U.S. Air Force and Navy, NASA,

industry, and tunnels in three Western European countries - the United Kingdom, France, and the Netherlands. The cone became known as the AEDC 10-deg Transition Cone, tested as a standard calibration body in 23 different wind tunnels.

The overall investigation which has been undertaken is comprised of two parts, (1) tunnel-to-tunnel correlation and (2) tunnel-to-flight correlations. The first part has been completed, and the purpose of this report is to document the results of the transition experiments conducted in the 23 wind tunnels.

It is planned that this cone will be flight tested at NASA's Dryden Flight Research Center as a joint venture undertaken by the USAF and NASA. The instrumentation is to be the same as described in this report in order that comparative data might be obtained between wind tunnels and free flight.

This volume (Volume I) is a documentation of the experimental methods used during the course of this investigation together with a summary of the important results obtained. Volume II contains a detailed presentation of the data from each wind tunnel.

2.0 CONE MODEL

2.1 PHYSICAL CHARACTERISTICS

A sketch of the AEDC 10-deg Transition Cone with primary instrumentation locations is shown in Fig. 1a. The cone has a 10-deg included angle (5-deg half-angle) and overall length of finished surface of 36 in. The tip bluntness is less than 0.005-in. equivalent diameter. The tip condition and surface finish were considered to be the two most important geometric features in the experiment as the body shape was conical with a surface true within about ±0.006 deg. There have been three incidences in which the cone tip was accidentally bent during installation in wind tunnels. Each time it was

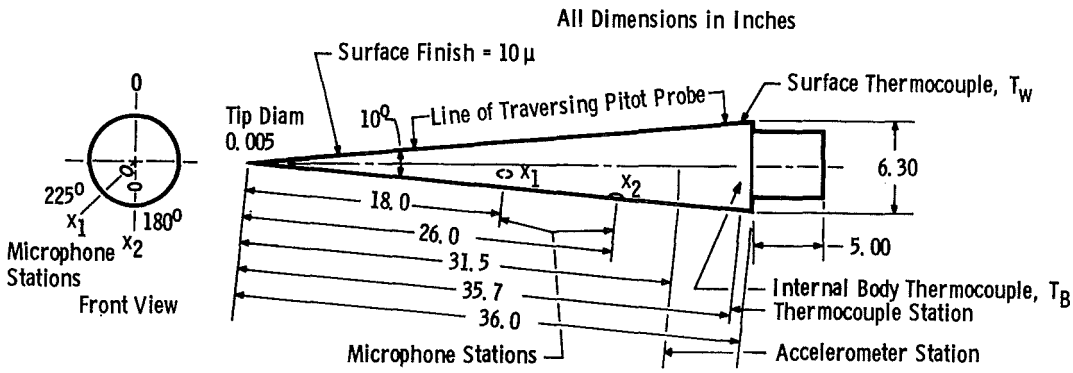

a. Primary instrument locations

Figure 1. AEDC 10-deg transition cone model.

possible to straighten the tip without breakage or any loss of metal. However, a slightly crooked tip shape was sustained as shown at about its worst after any test in the magnified photograph (Fig. 1b). There were two bends in the tip, one approximately 0.015 in. back from the apex and the other approximately 0.045 in. from the apex. While the extreme forward part of the cone tip was approximately aligned with the cone axis, a small length of the apex was slightly offset about 0.005 in. from the cone centerline because of the inability to perfectly straighten the tip. Typically, the tip was straightened to the condition shown in Fig. 1c. It had a very slight bend in the 90-deg orientation approximately 0.012 in. back from the apex with no offset.

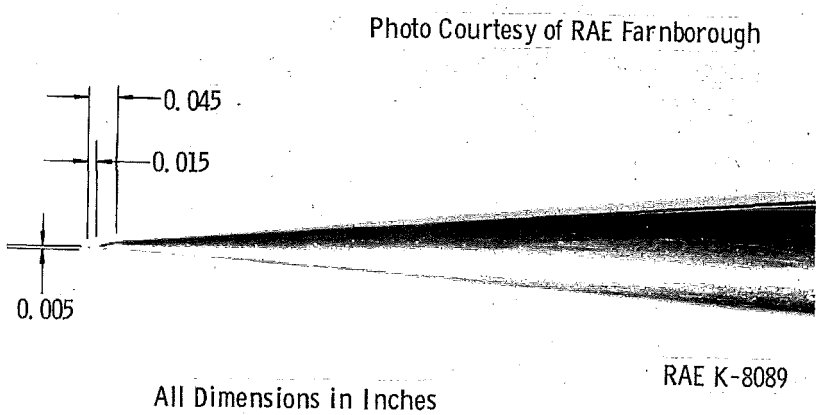

b. Worst-case tip detail
Figure 1. Continued.

The cone was fabricated from two pieces of 17-4 stainless steel, assembled, finish ground, and hand polished to the final surface finish of nominally 10-μin. rms. The finish has been checked repeatedly between tests using a surface profilometer with a diamond-point stylus of 500-μin. radius. Profilometer readings have varied over a range from approximately 5 μin. to approximately 15 μin. during these checks. On some occasions, the surface has been repolished using wet surface abrasives followed by dry applications of fine-grain polish and jeweler's rouge. Before each test, the cone surface was given a thorough cleaning to remove any dust particles or oily substances including fingerprints deposited in handling. The joint between the two pieces was located at approximately 12 in. from the apex where a 3/8-in.-diam locking pin extends through from surface to surface on the 90-270 deg axis. The joint and pin were polished to the extent that their existence was detectable only by microscopic examination.

Transition data were acquired on the 0-deg ray using a traversing pitot probe which was maintained in contact with the surface. Transition was also detected from observing the amplitude and frequency characteristics of the microphone signals. One microphone was located at x_1 = 18 in. from the apex on the 225-deg ray. The other microphone was

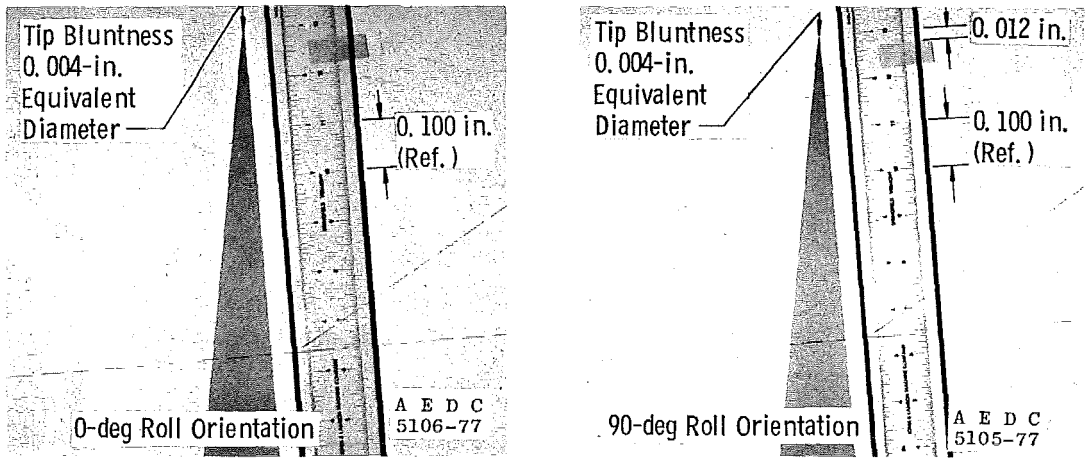

c. Final tip condition
Figure 1. Concluded.

located at x_2 = 26 in. from the apex on the 180-deg ray. The cone was sting-mounted in wind tunnels in either of two configurations, (1) with the cone extension and flow angularity probe or (2) with the dummy strut. Descriptions of these two configurations follow.

The traversing pitot probe was operated by a rack-and-pinion gear drive system which mounted to a 3-ft-long sting behind the cone. Although the probe and strut were designed to minimize interference, a dummy strut (Fig. 2a) with geometry similar to that of the traverse mechanism was used for much of the testing to provide symmetry of flow over the cone. The dummy strut was sometimes removed to make room for a flow angularity probe (Fig. 2b) required for measurements of the cone incidence angle during future flight tests.

A cone extension section (Fig. 2b) increased the overall body length to 44.5 in. The cone extension was added to the model with the flow angularity probe to move the base expansion wave influence at supersonic speeds aft and away from the flow angularity probe, and to lessen the influence of the base expansion on the cone surface pressure gradient at subsonic speeds.

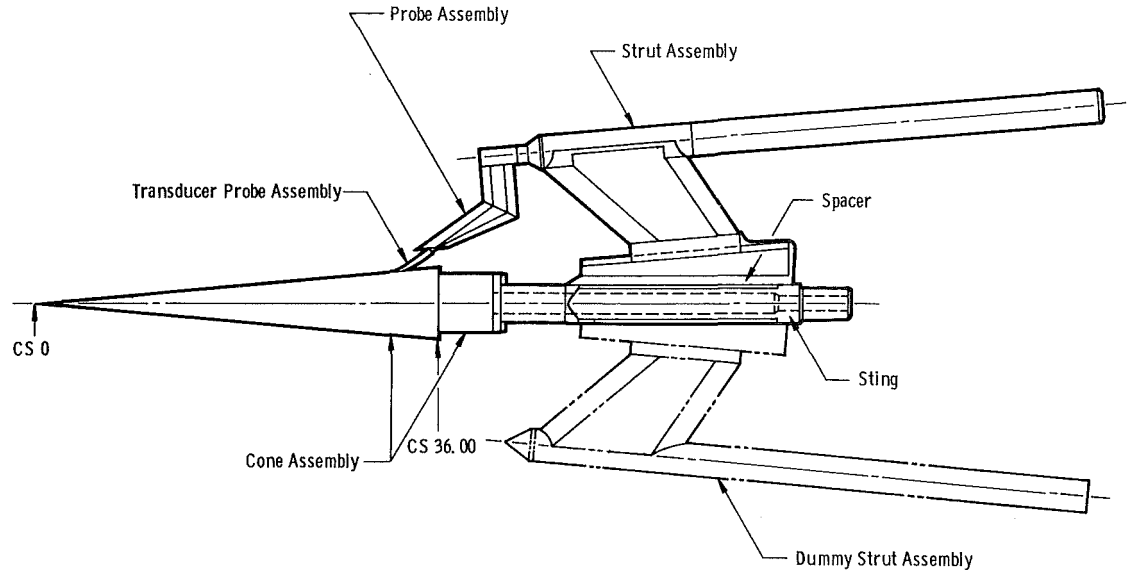

a. Configuration with dummy strut

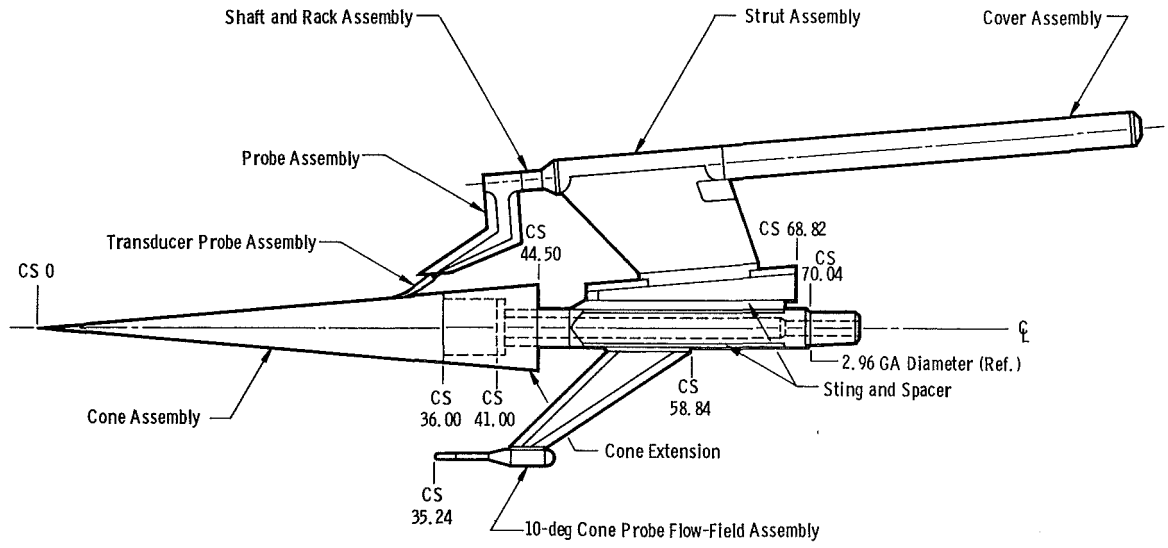

b. Configuration with flow angle probe and cone extension

Figure 2. Pitot pressure probe installation sketch.

2.2 INSTRUMENTATION AND CALIBRATION PROCEDURES

There were up to seven sensing instruments mounted inside the cone body. Measurements were also made of the external traversing pitot probe pressure and position.

Traversing Pitot Probe

The traversing pitot pressure probe and its support strut are shown schematically in Fig. 3a. Two of the four probes fabricated for these experiments are shown in the photograph in Fig. 3b. Also shown is the Kulite® Model CQL-125-5 1/8-in.-diam strain-gage-type pressure transducer. The transducer had temperature compensation to minimize distortions over an approximate temperature range of 0 to 180°F. The transducer cavity was sealed with an O-ring (Fig. 3a) and the reference line routed to a free-stream static source such that the transducer measured a differential between local total pressure at the sensing tube opening and the free-stream static pressure.

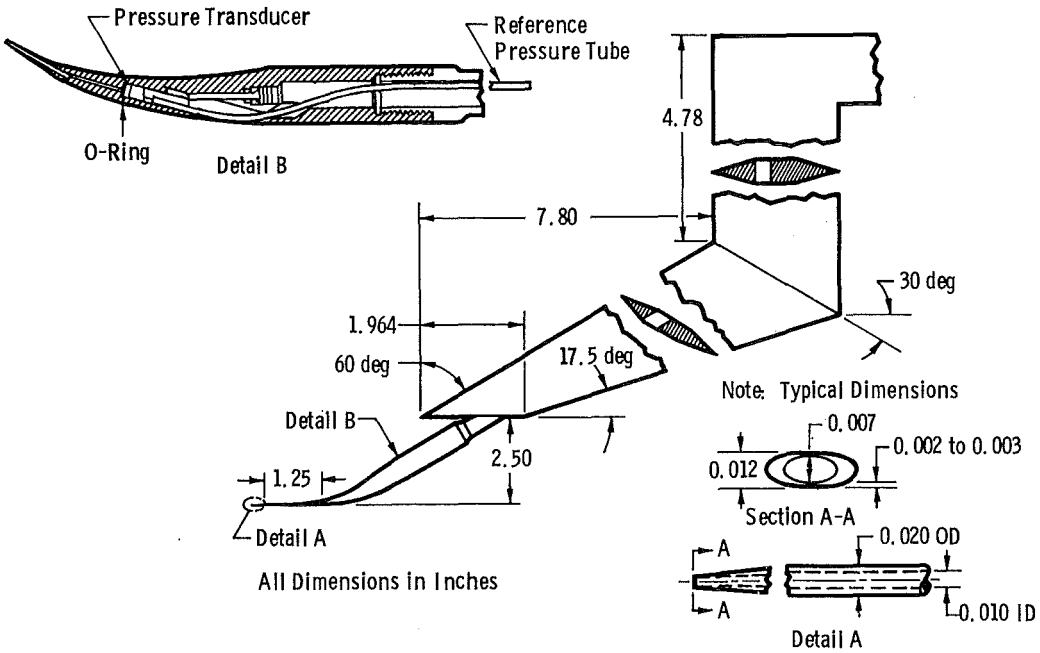

a. Schematic diagram

Figure 3. Details of pitot pressure probe assembly.

The pitot probe heads were fabricated from 0.020-in.-OD stainless steel hyperdermic needles stiffened with stainless steel sleeves soldered over the sensing tube to form a smooth transition in frontal area to the probe body which housed the transducer. The transducer was closed-coupled with as short a sensing tube length as practical. The tip of the sensing tube was flattened to an opening height of nominally 0.006 in. The probes were used interchangeably, but some of the probes after normal wear were measured posttest to have as much as 0.009- in. opening height. A typical sensing tube tip opening is shown in the photograph in Fig. 3c. These were continually refurbished in the effort to maintain a minimum practical tip opening height of 0.004 in. This 0.004-in. limit was imposed by the manufacturing techniques employed.

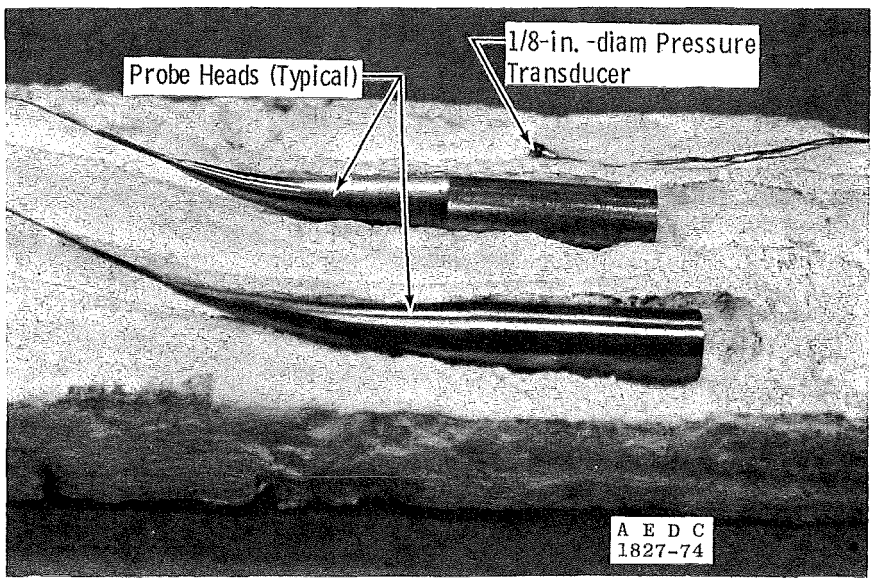

b. Photograph of probes and transducer
Figure 3. Continued.

The sensing tube was contoured in such a way as to give spring tension against the cone surface. The spring tension feature compensated for slight misalignment or relative vibratory motion between the traverse mechanism and cone during traverse of the cone length. Alignment of the probe to the cone was a critical factor in the validity of the transition data in that it was essential that the sensing tube remain in contact with the cone surface.

The pressure transducer was calibrated before each test under wind-off conditions by applying discrete changes in reference back pressure. Each pitot probe/transducer combination was calibrated dynamically in the laboratory by measuring response times under step changes in input pressure. A typical dynamic calibration revealed a frequency response down 3 db at 30 Hz. The calibration is included in Fig. 4 for record purposes.

The pitot pressure transducer signal was split into two outputs, separately filtered and amplified. One output was essentially a steady-state reading using a 2-Hz low-pass filter. The other signal was high-pass filtered at 2 Hz and conditioned through an rms-to-d-c converter. The dynamic output signal represented a time-averaged (over 3 sec) rms level of fluctuations in the bandwidth shown in Fig. 4. The two signals, steady state and dynamic, each provided information on location of certain significant points in the transition process.

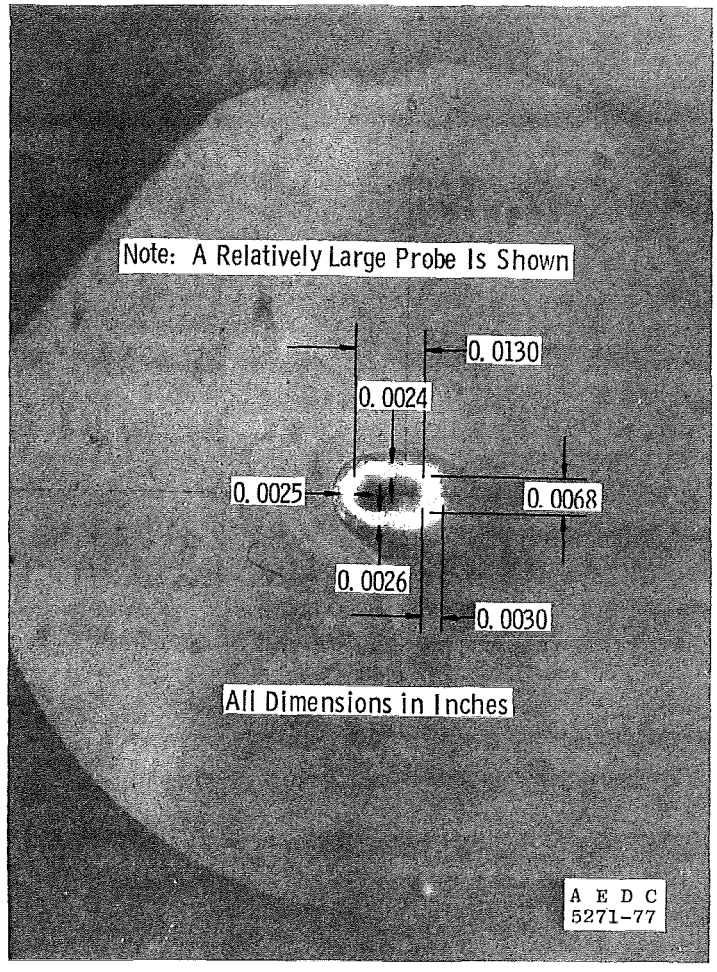

c. Microscopic photograph of a typical probe opening

Figure 3. Concluded.

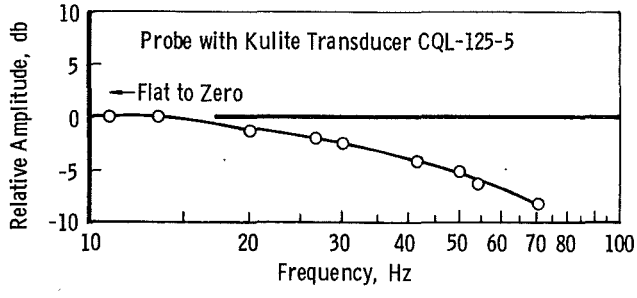

Figure 4. Typical pitot pressure probe sensing tube/transducer frequency response.

A ten-turn, 0- to 20-volt d-c Spiralpot® potentiometer was used to measure the location of the sensing tube opening along the cone surface. The potentiometer was driven through a gear reducer coupling in the traverse drive mechanism and calibrated from 0 to 33.5 in. along the actual cone surface length (5-deg half-angle) from the cone apex. Position calibrations were repeated pretest and posttest and were estimated to be repeatable to approximately ±0.05 in.

Microphones

Two Bruel and Kjaer 1/4-in.-diam Model 4136 condenser-type microphones were used to measure surface static pressure fluctuations approximately 18 and 26 in. from the cone tip. These measurements were made to establish the level of free-stream disturbances actually reaching the cone in order that transition Reynolds number might be correlated with the level of free-stream disturbance in a wind tunnel. The microphone diaphragms were positioned flush with the cone surface as shown in Fig. 5a, making use of either a

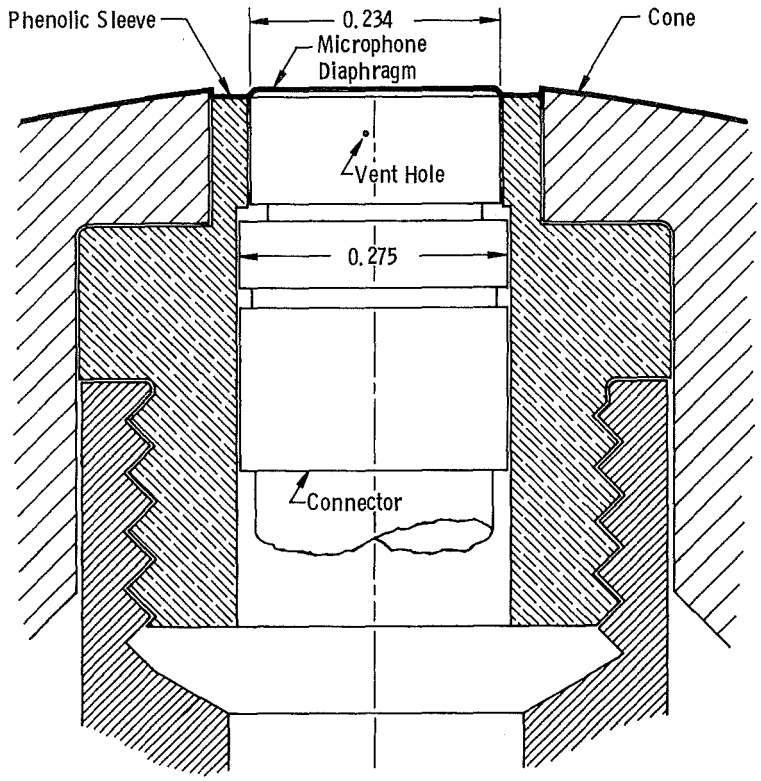

a. Microphone installation details at X_1 = 18 in.

Figure 5. Details of microphone transducer installation in cone.

Teflon® or phenolic sleeve to isolate the microphone electrically and mechanically (from high-frequency vibrations). Bruel and Kjaer power supplies, amplifiers, and preamplifiers close-coupled inside the cone were used as a matched system for best signal recording fidelity.

There were tests in which Kulite 1/8-in.-diam strain-gage-type transducers were used rather than the condenser microphones. The transducers were Type CQL-125-5, mounted in phenolic sleeves as shown in Fig. 5b. The condenser microphones had better sensitivity (greater dynamic range) than the strain-gage transducers and became the standard instrumentation.

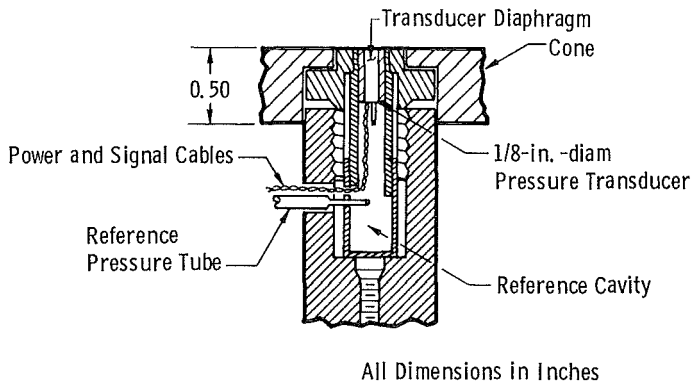

b. Transducer installation details at X_1 = 18 in.
Figure 5. Concluded.

The frequency response of the microphone was different from that of the transducer and also varied with cable length which was different from tunnel to tunnel. Both systems were probably flat in all cases to at least 20 kHz. Frequency response was documented more carefully for the 1/4-in. microphones than for the 1/8-in. transducers, the smaller transducers having the higher frequency response. Typical microphone calibration data from the installation in the AEDC 16-ft Transonic Propulsion Wind Tunnel (16T) (Tunnel 16T) are shown in Fig. 6. Two curves are shown in Fig. 6, the first representing the manufacturer's published data for the microphone alone (Ref. 11), and the second containing the attenuation inherent in the transmission cables for the AEDC Tunnel 16T installation. The cable lengths were approximately 300 ft in this case. This second curve in Fig. 6 is flat within ±1 db from 40 Hz to 50 kHz for ambient pressure and temperature, wind off.

There is a very strong influence of absolute pressure on the Bruel and Kjaer 4136 microphone frequency response at pressure levels lower than one atmosphere. This influence is shown typically in Fig. 7 for the microphone alone (Ref. 11). At

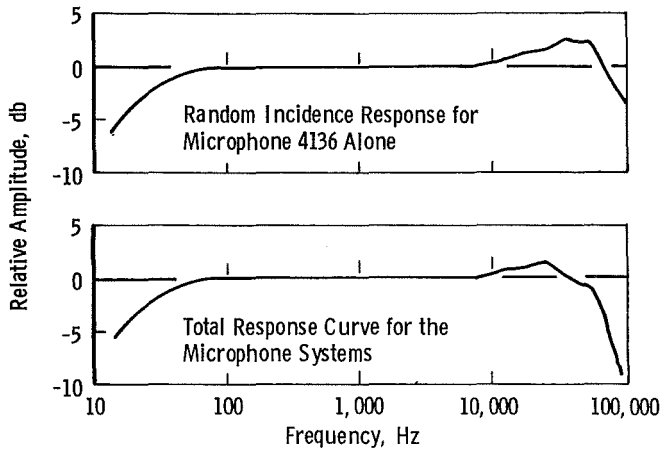

Figure 6. Typical measured frequency response for installed microphones.

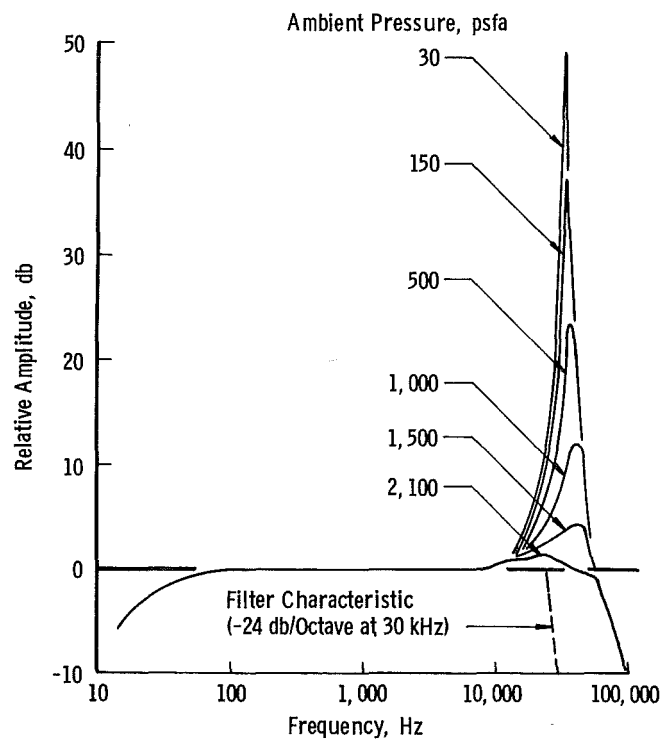

Figure 7. Influence of absolute pressure level on microphone frequency response.

low-pressure levels the microphone response changes drastically because of the change in mechanical damping with a shift in diaphragm resonant frequency from approximately 76 kHz to approximately 48 kHz as indicated in Fig. 7. The low free-stream static pressure

in supersonic tunnels for Mach numbers greater than about 1.5 is usually sufficient for the resonant frequency to approach 48 kHz with very large signal amplification resulting.

The overall root-mean-square amplitude was recorded in some cases without filters on a true root-mean-square voltmeter capable of frequency response to at least 250 kHz. In these cases, large errors were introduced because of the diaphragm resonance. A set of calibrations was performed in the AEDC Tunnel 16T to M_∞ = 1.5 and in the NASA/Langley 4-ft Supersonic Unitary Plan Wind Tunnel Test Section No. 2 (NASA/Langley 4 SUPWT TS No. 2) at M_∞ = 3.5 and 4.6 to derive corrections for the unfiltered data. Additional data relative to this problem with the same type microphone are given by Pate and Brown in Ref. 8. The calibrations were made using a variable low-pass filter adjusted from 2 kHz to 250 kHz at each (constant) flow condition. By measuring the accumulated overall rms output from the microphone at each filter setting, a frequency response curve could be generated in terms of the output signal (given in volts, rms). Typical data obtained in these calibrations are shown in Fig. 8 at M_∞ = 3.51 and 4.60. The conditions tested represented a variety of boundary-layer flow conditions

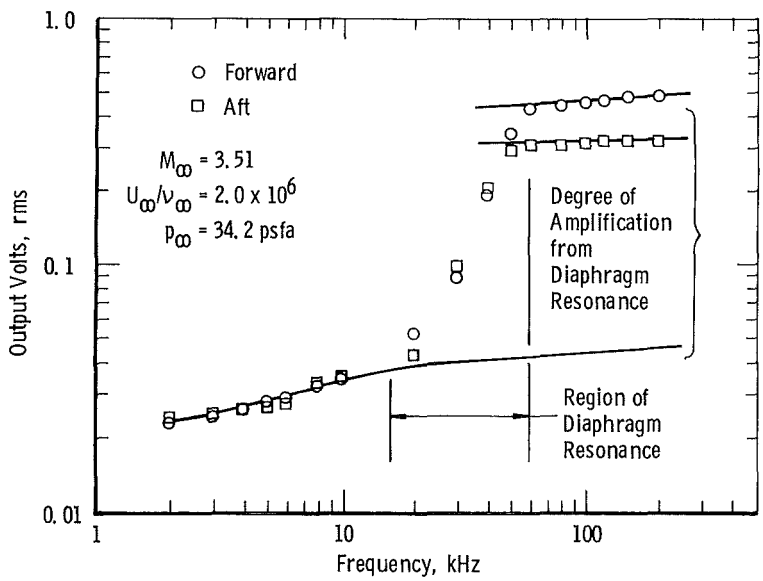

a. M_∞ = 3.51

Figure 8. Effect of microphone frequency response on typical fluctuating pressure rms levels.

over the two cone microphones: laminar, turbulent, and transitional (Reference Volume II). However, the amount of amplitude increase measured near 48-kHz frequency was roughly the same at all different boundary-layer conditions. The method of deriving an overall amplitude correction factor was to shift the trend curves downward in

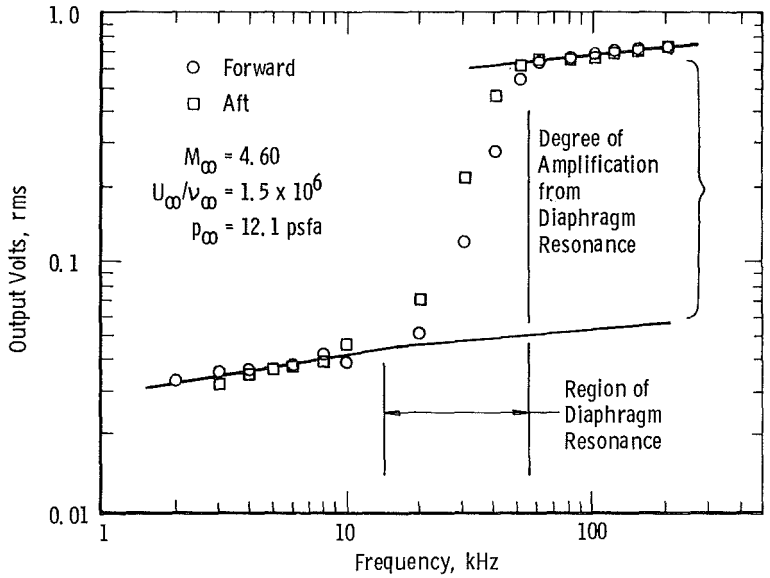

b. M_∞ = 4.60

Figure 8. Concluded.

accumulated rms level above the resonant frequency to match those below the resonance, thus reconstructing an accumulated rms curve as if there had been no resonance. The ratio of final accumulated rms levels, with and without the resonance, was then defined as the correction factor. Correction factors thus derived are given in Table 1 after taking an average between those for the two microphones at each flow condition. The resulting faired curve through the data is shown in Fig. 9.

Table 1. Correction Factors for Microphone Frequency Response

TUNNEL	M_∞	$U_\infty/\nu_\infty \times 10^{-6}$	p_∞, psfa	Correction Factor
NASA/Langley 4 SUPWT	4.6	1.0	8.1	0.102
	4.6	1.5	12.1	0.066
	3.5	1.0	17.1	0.277
	3.5	2.0	34.2	0.127/0.188
	3.5	3.5	59.7	0.194
AEDC 16T	1.6	1.4	165	0.800
	1.6	1.9	235	0.880
	1.6	3.0	377	0.911
	1.5	1.4	191	0.838
	1.5	2.0	272	0.914
	1.4	1.0	141	0.815
	1.4	1.4	220	0.867
	1.4	2.0	314	0.895

Data were recorded in the NASA/Langley 4-ft Supersonic Pressure Tunnel (NASA/Langley 4 SPT) and the NASA/Langley 4 SUPWT TS No. 1, the Royal Aircraft Establishment 8- x 8-ft Supersonic Wind Tunnel and the 3- x 4-ft High Speed Supersonic Tunnel at Bedford, England (RAE Bedford 8 x 8 SWT and 3 x 4 HSST) without filters and later corrected using the factors shown in Fig. 9. Data taken at $M_\infty \geq 1.4$ were also corrected in the AEDC Tunnel 16T. All other data used were uncorrected.

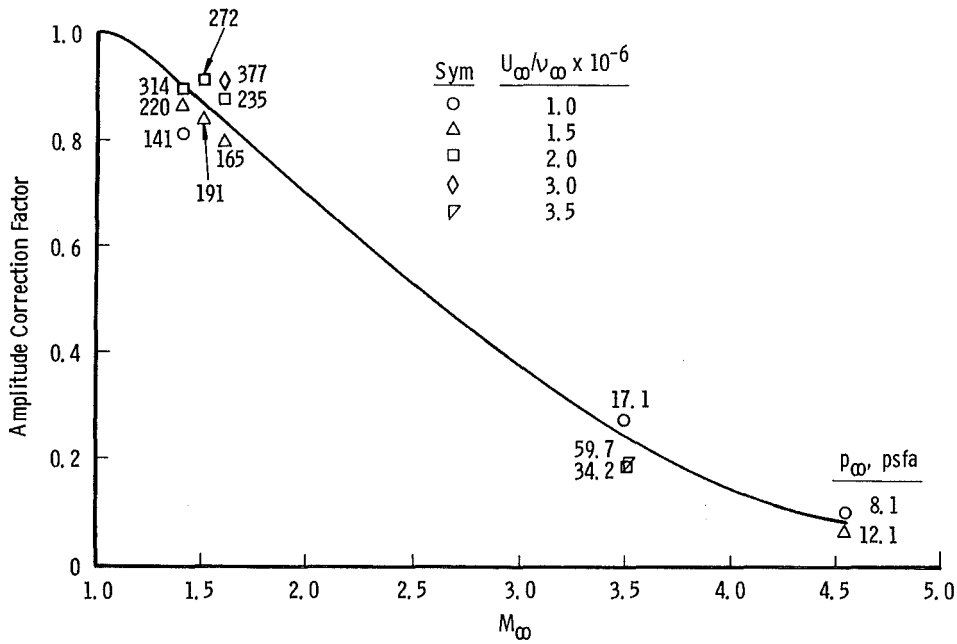

Figure 9. Correction factors for microphone frequency response effects on output amplitudes.

For some of the tests in supersonic tunnels, a compromise technique was adopted of low-pass filtering the microphone signals to eliminate the need for large after-the-fact corrections. The filters were set at 30 kHz throughout these tests. The 30-kHz filters were used in the NASA/Ames Research Center 9 x 7 Supersonic Wind Tunnel (NASA/Ames 9 x 7 SWT) and the NASA/Langley 4 SUPWT TS No. 2.

Routine calibrations of the microphones and transducers were performed pretest and posttest using a direct-coupled pistonphone (see Fig. 10). A sinusoidal calibration signal at 1 kHz was applied to the microphone using a calibration fixture to seal the pistonphone cavity in a precise orientation over the diaphragm with an O-ring seal. The calibration level was adjustable at 140, 150, or 160 ± 0.5 db (Ref. 0.0002 dynes/cm^2). All three calibration levels were used in order to make periodic linearity assessment of microphone output.

The manufacturer's stated acceleration sensitivity for the microphones is maximum in the axis perpendicular to the diaphragm and is 88 db for an acceleration level of 1-g rms. This is a very low value, equivalent to 0.011-psf rms, and is mainly determined by the mass of the diaphragm. Less precise knowledge was available regarding acceleration sensitivity of the mounted pressure transducers.

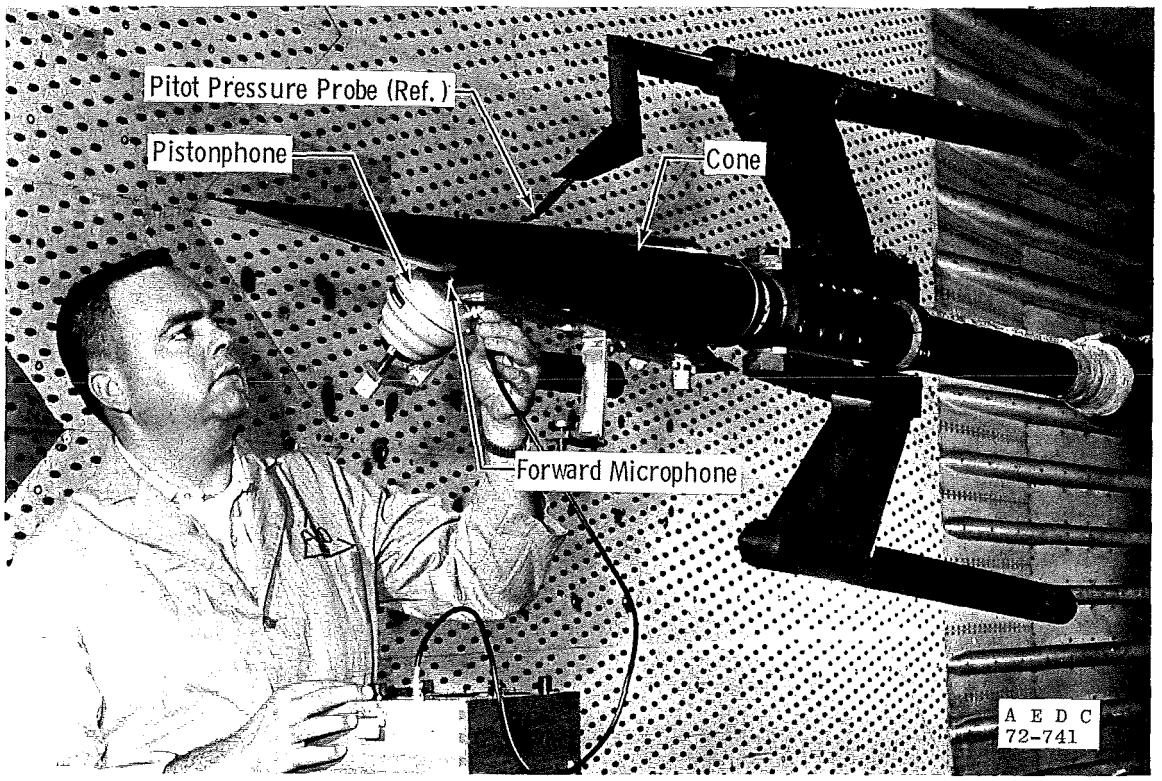

Figure 10. Cone model installation photograph during microphone calibration in AEDC PWT Tunnel 16T.

Accelerometers

An Endevco Model 2211 piezoelectric accelerometer was used in most of the wind tunnel tests mounted inside the cone, 31.5 in. from the apex, in an axis perpendicular to the diaphragm of the aft microphone. The purpose of this accelerometer was to provide a means for assessing acceleration sensitivity of the microphone signals. A triaxial package using miniature Entran Model EGAL-125-30 strain-gage transducers was installed only for the tests in the NASA/Ames 11-ft Transonic Wind Tunnel (NASA/Ames 11 TWT), at Sta 133 in., and the NASA/Ames 9 x 7 SWT. The flat frequency response range was from approximately 3 Hz to 300 Hz. There were mounting block and/or other internal

component resonances near 2 kHz and 4 kHz. Acceleration signals were recorded at up to 10 kHz, recognizing their limitations in usable frequency range.

The overall levels of acceleration measured by the cone accelerometers were documented at the same time as the ΔC_p measurements, and spectral analyses were likewise performed on the acceleration data. Noise levels, in general, greatly exceeded the threshold level for microphone acceleration sensitivity; at no time did it become necessary to correct any of the microphone data for acceleration sensitivity.

Flow Angularity Probe

The flow angularity probe was installed in order that its sensitivity and position error calibrations might be obtained for future flight tests at the same time that effects of incidence angle on transition were being measured.

The probe had a hemispherically shaped head containing five 0.020-in.-diam orifices, one at the 0-deg angle-of-attack stagnation point, a pair at 40 deg from this stagnation point to measure angle of attack, α, and a pair at 40 deg to measure yaw angle, β. The angles α and β were determined from the differential pressure between orifice pairs. There was a static pressure ring on the cylindrical portion of the probe to serve as a static pressure reference source. There was also a static pressure ring on the cone extension at 42.5 in. distance from the cone apex. Both static pressure rings had four mutually perpendicular orifices on the same axial circumference. The four readings were averaged in order to eliminate any effects of incidence angle.

Surface and Body Thermocouples

A copper-constantan thermocouple was installed just beneath the surface 35.7 in. from the apex to estimate when the cone came into thermal equilibrium with the wind tunnel flow. An iron-constantan thermocouple was attached to the cone interior and was also monitored as a function of time to determine the lag of the cone mass approaching equilibrium temperature.

3.0 FACILITIES

The facilities included in this investigation are discussed briefly in the context of noting distinguishing geometric factors (see Table 2) which are referred to in the discussion of results. For further details on a particular facility, the reader is referred to appropriate brochures, users' guides, or tunnel calibration reports available from the appropriate tunnel of interest.

Table 2. Summary of Wind Tunnel Characteristics

Group	Tunnel	Distinguishing Geometry	Mach Number Range	Unit Reynolds Number Range x 10^{-6}	Predominant Disturbances	Resonant Mach Number	ΔC_{pmax}, %
1	NASA/Langley 8 TPT	Slotted Wall	0.25 - 1.20	2.0 - 3.0	Low Frequency	0.80	2.20
	NASA/Langley 16 TT	Slotted Wall	0.20 - 1.30	1.3 - 3.9	Low Frequency	0.82	3.60
	NASA/Langley 16 TDT (Freon)[1]	Slotted Wall	0.30 - 1.15	1.5 - 3.7	Low Frequency	0.85	1.40
	NSR&DC 7 x 10 T	Slotted Wall	0.20 - 1.13	1.5 - 4.0	Low Frequency	0.75	1.26
	NLR 6.55 x 5.28 HST[2]	Slotted Wall	0.15 - 1.30	1.5 - 1.4	Compressor	0.80	1.01
	RAE Farnborough 8 x 6[3,6]	Slotted Wall	0.20 - 1.19	0.4 - 2.5	Compressor	0.60	1.90
	NASA/Ames 12 PT	Solid Wall	0.20 - 0.90	2.0 - 3.0	Test Section	0.65	1.65
	RAE Bedford 8 x 8 SWT (Subsonic Mode)	Solid Wall	0.20 - 0.80	0.25 - 3.0	---	none	0.80
2	AEDC Tunnel 4T	Perforated Wall	0.40 - 1.30	1.5 - 5.0	Edgetones	0.80/1.30	3.75
	ONERA 6 x 6 S-2 Modane	Perforated Wall	0.25 - 1.30	2.0 - 7.2	Edgetones	0.80	2.77
	ONERA 2.56 x 1.83 S-3 Modane[2,6]	Perforated Wall	0.25 - 1.00	2.0 - 12.5	Stilling Chamber	0.25	12.7
	AEDC Tunnel 16T	Perforated Wall	0.20 - 1.60	1.0 - 5.6	Edgetones	0.71	2.68
	NASA/Ames 11 TWT	Corrugated-Slot Wall	0.40 - 1.20	1.5 - 6.0	Slot Organ Pipe	0.75	2.00
	NASA/Ames 14 TWT	Corrugated-Slot Wall	0.40 - 1.05	2.6 - 4.0	Slot Organ Pipe	0.95	2.05
	Calspan 8 TWT	Perforated Wall	0.60 - 0.95	2.0 - 3.0	Wall Tones	0.85	2.10
	ARA, Ltd. Bedford 9 x 8[4]	Perforated Wall	0.21 - 1.40	1.5 - 4.4	Wall Tones	0.68	2.65
3	RAE Bedford 8 x 8 SWT[5]	Converg/Diverg Nozzle	1.40 - 2.40	0.6 - 4.0	Wall Boundary Layer	None	0.45
	NASA/Langley 4 SPT	Converg/Diverg Nozzle	1.61 - 2.01	1.0 - 5.0	Wall Boundary Layer	None	0.12
	AEDC Tunnel 16S[6]	Converg/Diverg Nozzle	1.67 - 2.20	0.9 - 2.2	Wall Boundary Layer	None	0.50
	AEDC VKF Tunnel A	Converg/Diverg Nozzle	1.51 - 5.50	2.3 - 6.8	Wall Boundary Layer	None	---
	RAE Bedford 3 x 4 HSST	Converg/Diverg Nozzle	2.50 - 4.50	0.7 - 9.2	Wall Boundary Layer	None	0.20
4	NASA/Ames 9 x 7 SWT	Sliding-Block Nozzle	1.50 - 2.50	2.0 - 4.5	Wall Boundary Layer	None	0.18
	NASA/Langley 4 SUPWT (TS No. 1)	Sliding-Block Nozzle	1.60 - 2.86	1.5 - 5.0	Wall Boundary Layer	None	0.14
	NASA/Langley 4 SUPWT (TS No. 2)	Sliding-Block Nozzle	2.86 - 4.60	1.5 - 6.5	Wall Boundary Layer	None	0.24

[1] Tests performed using both Freon and air as tunnel working fluid

[2] Only noise data, no transition data

[3] Results affected by model surface imperfections during this test

[4] Transition data at Mach numbers from 0.2 to 0.6 only

[5] Data acquired in Mach number range from 0.2 to 0.8 also

[6] Data not included in Volume I but presented in Volume II

The number of tunnels selected for this experimental study was exceedingly large, covering a broad range of Mach numbers, Reynolds numbers, sizes, and geometrical configurations. This was made possible by the general nature of the research being performed and the spirit of cooperation between the U.S. Air Force, NASA, the U.S. Navy, industry, and the governments of the three participating Western European countries.

The organization of the facilities into specific groupings is germane to the results of the experiments and their logical presentation in this report. While this particular grouping will be an aid to the understanding of the boundary-layer transition results on this particular cone, it should not be construed as a general classification for all types of aerodynamic testing that may be performed in these tunnels.

3.1 GROUP 1 - SUBSONIC AND TRANSONIC, SLOTTED

Group 1 contains a particular class of transonic tunnels, distinguished by their coarsely spaced slotted test section design with nominally 4.5- to 5.0-percent open area, and solid-wall subsonic tunnels. There is one exclusively subsonic tunnel, the NASA/Ames Research Center 12-ft Pressure Tunnel (NASA/Ames 12 PT). One other tunnel, the RAE Bedford 8 x 8 SWT, also in Group 3, could be operated at both supersonic and subsonic speeds, providing additional solid-wall subsonic tunnel data to complement those from the NASA/Ames 12 PT.

There were six slotted-wall transonic tunnels. The three NASA/Langley Research Center Transonic Tunnels, 8-ft Transonic Pressure Tunnel (8 TPT), 16-ft Transonic Tunnel (16 TT), and 16-ft Transonic Dynamics Tunnel (16 TDT), are distinguished by a tapered slot design contoured for optimized axial Mach number distribution. The Naval Ship Research and Development Center 7- x 10-ft Transonic Tunnel (NSR&DC 7 x 10 T) has a test section with slot design similar to the Langley tunnels. The NASA/Langley 8 TPT has slotted top and bottom walls with solid side walls. The NASA/Langley 16 TT has an octagonal test section with eight slots. The NASA/Langley 16 TDT has the slotted top and bottom walls but incorporates additional vents (of different contour to the basic tapered slot) in the two side walls. The NSR&DC 7 x 10 T has slotted 10-ft top and bottom walls and solid 7-ft side walls. The NLR 6.55- x 5.28-ft high-speed tunnel at Amsterdam (NLR 6.55 x 5.28 HST) has slotted top and bottom walls with solid side walls. The Royal Aircraft Establishment 8- x 6-ft Transonic Tunnel at Farnborough, England (RAE Farnborough 8 x 6) has a test section with all four walls slotted with a different slot contour and width. This tunnel has a unique feature among all those included in this investigation in its annular-return circuit. The annular-return circuit represents a very compact design concept; however, the fan poses a strong noise source located very close behind the test article at the exit to the diffuser.

The NASA/Ames 12 PT is a subsonic tunnel with a cylindrical test section of solid-wall design. The upper limit Mach number with the cone installed was 0.95. The RAE Bedford 8 x 8 SWT could be operated over the Mach number range from 0.2 to 0.8 as well as the range from 1.4 to 2.4.

These eight tunnels have been grouped together because of relatively lower test section noise levels, compared to the tunnels of Group 2. This lower sound generation is attributable primarily to the test section design. All of the tunnels of Group 1 with the exception of the NASA/Langley 16 TT have variable density capability. The NASA/Langley 16 TT is an atmospheric tunnel. The NASA/Langley 16 TDT is unique among all of the tunnels in this investigation in its ability to use either air or Freon as the working fluid medium.

3.2 GROUP 2 - TRANSONIC, POROUS

The eight tunnels in Group 2 are all transonic facilities distinguished by higher test section noise levels relative to Group 1 and by test section wall design with the goal to attenuate shock and expansion waves.

There are three basic test section wall designs represented in the tunnels of Group 2: (1) The perforated wall with 60-deg inclined holes, which provide differential resistance between inflow and outflow. These have porous open areas of nominally six percent, but sometimes variable porosity from as low as 0.5 percent to as much as 30 percent. (2) The normal-hole perforated wall with nominally 22.5-percent porous open area. (3) The finely spaced slotted wall with corrugated-insert slot baffles and nominally 5.6-percent porous open area.

Perforated-wall tunnels using the 60-deg inclined-hole configuration are the AEDC 4-ft Aerodynamic Wind Tunnel 4T (Tunnel 4T), the ONERA 6- x 6-ft S-2 MA Facility at Modane, France (ONERA 6 x 6 S-2 Modane), the ONERA 2.56- x 1.83-ft S-3 MA Facility at Modane (ONERA 2.56 x 1.83 S-3 Modane), and the AEDC Tunnel 16T. The ONERA S-3 facility can be operated in either transonic or supersonic modes using either perforated or solid test section walls, respectively. This facility is the only blowdown-type tunnel in which the cone was tested. The ONERA S-2 Facility is similar in design to the AEDC Tunnel 4T in that both have a variable porosity feature, using sliding cutoff backing plates to vary porosity from zero to six percent. However, the ONERA S-2 facility has only top and bottom walls perforated with solid side walls, whereas the AEDC Tunnel 4T has all four walls perforated. A fixed six-percent porosity is used in the AEDC Tunnel 16T, all four walls being perforated.

The Calspan 8-ft Transonic Wind Tunnel (Calspan 8 TWT) and the Aircraft Research Association, Ltd., 9- x 8-ft Transonic Tunnel at Bedford, England (ARA, Ltd. Bedford 9

x 8) are similar in design in that both utilize the 22.5-percent normal-hole wall, all four walls being perforated. Both test sections use an identical hole pattern having 0.50-in.-diam holes; however, the Calspan 8 TWT has a wall thickness of 0.50 in. and the ARA, Ltd. Bedford 9 x 8 has a wall thickness of 0.187 in. The Calspan 8 TWT is a variable density tunnel, but the ARA, Ltd. Bedford 9 x 8 is limited to total pressures close to atmospheric.

The NASA/Ames 11 TWT and the NASA/Ames 14-ft Transonic Wind Tunnel (NASA/Ames 14 TWT) have virtually identical test section design, different only in scale and only slightly in details of the baffle geometry in the finely spaced slots. All four walls have baffled slots in both tunnels. This wall design, in effect, combines some of the features of the purely perforated and the purely slotted designs but because of the higher test section noise levels is grouped with the perforated-wall tunnels. The NASA/Ames 11 TWT is a variable density tunnel; the NASA/Ames 14 TWT is an atmospheric tunnel.

3.3 GROUP 3 - SUPERSONIC, TWO-DIMENSIONAL

The five supersonic tunnels in Group 3 have solid test section walls and two-dimensional, variable geometry, converging-diverging nozzles. The range in Mach number covered in the tests performed in these tunnels was from 1.4 to 5.5. These tunnels are to be distinguished from the supersonic tunnels in Group 4 by the type of nozzle design.

The five tunnels of Group 3 are the RAE Bedford 8 x 8 SWT, the NASA/Langley 4 SPT, the AEDC 16-ft Supersonic Propulsion Wind Tunnel (Tunnel 16S), the AEDC von Kármán Facility 3.33- x 3.33-ft Supersonic Wind Tunnel (A) (Tunnel A), and the RAE Bedford 3 x 4 HSST.

3.4 GROUP 4 - SUPERSONIC, SLIDING BLOCK

The three supersonic tunnels of Group 4 have solid test section walls and variable geometry, sliding-block nozzles. The sliding-block nozzle is mechanically simpler than the two-dimensional, flexible-plate, converging-diverging nozzle of the Group 3 tunnels and is the distinguishing feature of the Group 4 tunnels.

The flow through the sliding-block-type nozzle takes a curved path from the stilling chamber into the test section introducing stream angularity to the flow in the test section. Using this type of nozzle, it is necessary to perform test section flow angle calibrations in order to determine a model pitch angle for zero relative flow incidence angle. The stream angle varies as a function of Mach number as the sliding block translates longitudinally.

The three tunnels which constitute Group 4 are the NASA/Ames 9 x 7 SWT and the two legs of the NASA/Langley 4 SUPWT, TS No. 1 and TS No. 2. The two test sections of the NASA/Langley 4 SUPWT are both nominally 4 ft square. The design of the NASA/Ames 9 x 7 SWT is very similar in all respects to the NASA/Langley 4 SUPWT having 7-ft vertical walls and 9-ft horizontal walls in the test section. In all Group 4 tunnels, the sliding block is located in the bottom horizontal wall of the nozzle such that zero incidence is obtained by pitching the model downward the proper amount to compensate for stream angle. The Mach number range covered by the tunnels of Group 4 was from 1.5 to 4.6.

4.0 EXPERIMENTAL METHODS

The basic objective in performing the experiments was to determine how transition Reynolds number on the cone varies with Mach number, unit Reynolds number, and noise level in wind tunnels. Therefore, it was important that the experimental methods employed be of a nature that could be repeated in a large number of wind tunnels. This dictated that experimental techniques be as simple as possible, that the instrumentation be standardized throughout the investigation, and that the defining parameters be as unambiguous as possible.

4.1 DEFINITION OF PARAMETERS

Free-stream Mach number (U_∞/a_∞) and unit Reynolds number (U_∞/ν_∞) were the primary independent variables of this investigation for the cone at zero incidence and in thermal equilibrium with the free-stream flow. The Mach number was determined to be repeatable within ±0.02 of the nominal value in virtually all tunnels. Unit Reynolds number was computed from measurements of free-stream total pressure (accurate to about ±4 psf), free-stream total temperature (accurate to about ±2°R), and free-stream Mach number.

All transition Reynolds numbers presented in this report are based upon the unit Reynolds number evaluated at free-stream conditions and an experimentally determined boundary-layer transition location measured from the cone apex. Various laminar-turbulent transition detection techniques give different views of the zone over which transition takes place, no two of them giving precise agreement on a definable transition point. The traversing pitot pressure probe had relatively high sensitivity to transition over the full range of M_∞ and U_∞/ν_∞ in the present investigation. It was relatively durable, and was extremely simple to use since it involved a single moving sensor as opposed to an array of multiple fixed sensors.

Some selected pitot pressure profile data and shadowgraph views of the cone boundary-layer transition at $M_\infty \approx 4.5$ are shown in Fig. 11. The most clearly definable point is the peak in pressure profiles denoted in Fig. 11a as x_T. As unit Reynolds number (U_∞/ν_∞) is reduced, the point x_T moves progressively further aft on the cone.

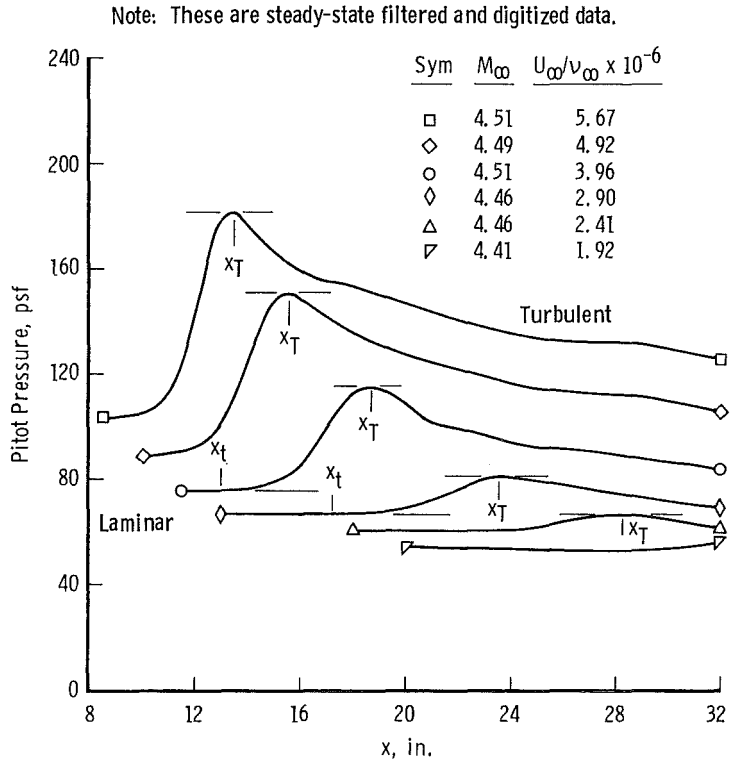

a. Pitot probe pressure

Figure 11. Typical pitot pressure probe data and shadowgraph views from AEDC VKF Tunnel A.

Likewise, there is a corresponding movement of the less clearly defined point denoted as x_t in these profiles. The shadowgraph views in Fig. 11b at corresponding test conditions show turbulent flow at U_∞/ν_∞ levels of 3.96×10^6 and 2.90×10^6, transitional flow at $U_\infty/\nu_\infty = 2.41 \times 10^6$, and laminar flow at $U_\infty/\nu_\infty = 1.92 \times 10^6$. The shadowgraph views show a small-scale turbulent eddy structure in the turbulent boundary-layer regions and thin (white) lacy lines which are approximately parallel to the cone surface in the laminar regions.

Some pitot pressure profile data taken to illustrate the movements of the transition zone with angle of attack, α, and angle of yaw, β, are shown in Fig. 12. Positive α placed the pitot probe on the leeward ray, where transition moved forward, and negative α on

the windward stagnation ray where transition moved aft. Yawing incidence provided measurements on the rays 90 deg from windward stagnation where there was a forward movement of transition essentially symmetrical for positive and negative β (negative β not shown).

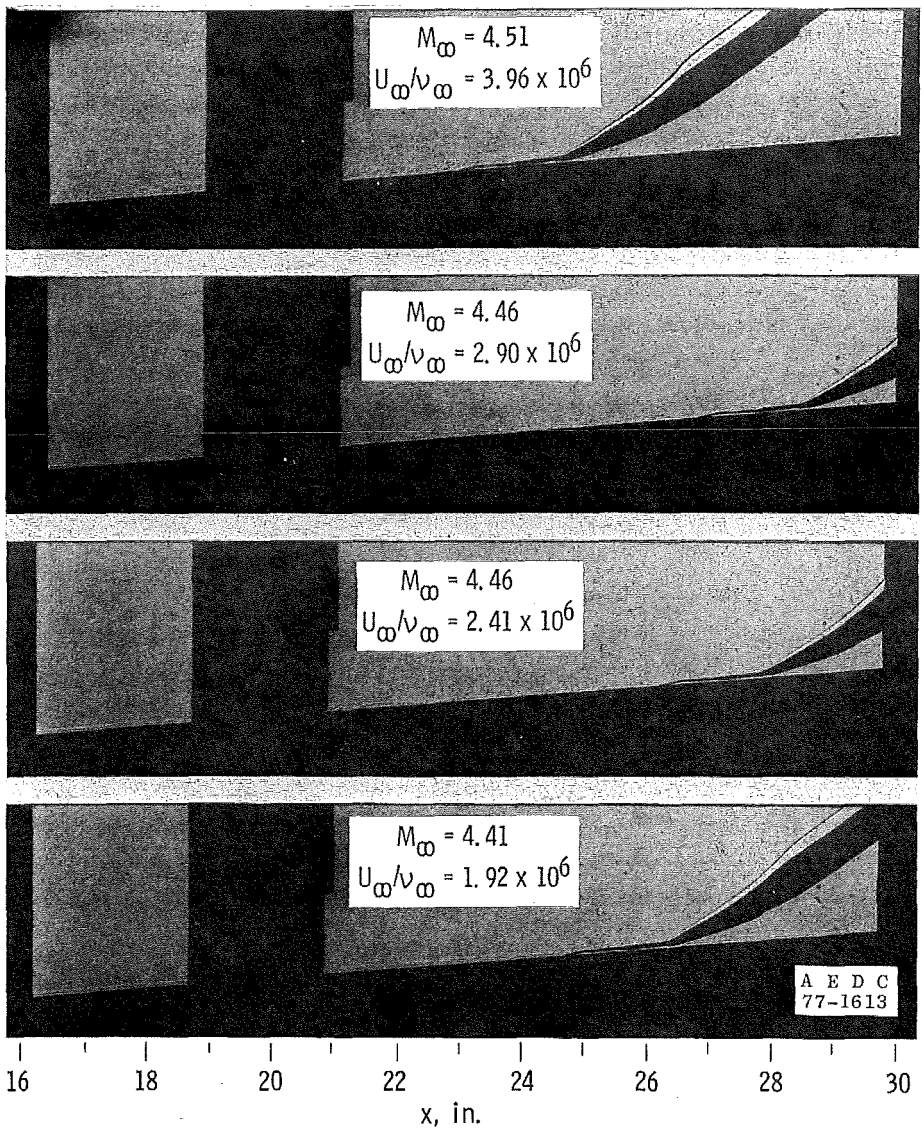

b. Shadowgraph views
Figure 11. Concluded.

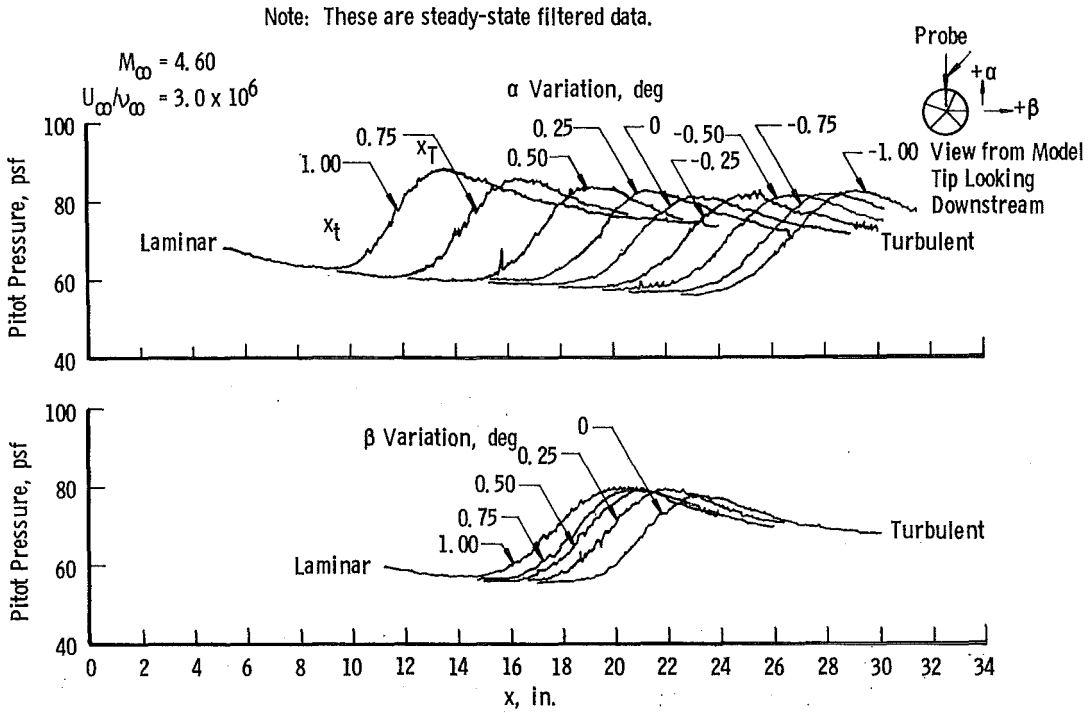

Figure 12. Typical variation of pitot pressure probe data with cone angle of attack and yaw.

As explained in Subsection 2.2, the pitot pressure transducer signal was split into two outputs, one being essentially the steady-state level of pressure and the other being the rms level of the dynamic signal. Enlarged analog traces of typical steady-state and rms fluctuation level (dynamic) outputs from the probe are shown in Fig. 13. The example given in Figs. 13a, b, and c are typical of profiles for high supersonic, low supersonic, and subsonic regimes of flow. All three figures are labeled with four distinguishable points in the profiles which will be defined in this report as roughly indicative of the following (see Fig. 13):

Location

a. First indications of departure from laminar trend,

b. Horizontal tangency to the profile minimum value which will be construed to lie close to the onset of transition (breakdown of laminar flow) and will be called x_t,

c. Peak in the rms fluctuation level corresponding closely to the inflection point in the steady-state profile to be called x_p, and

d. The maximum in the steady-state profile which will be construed to lie close to the end of transition (beginning of fully developed turbulent flow) and will be called x_T.

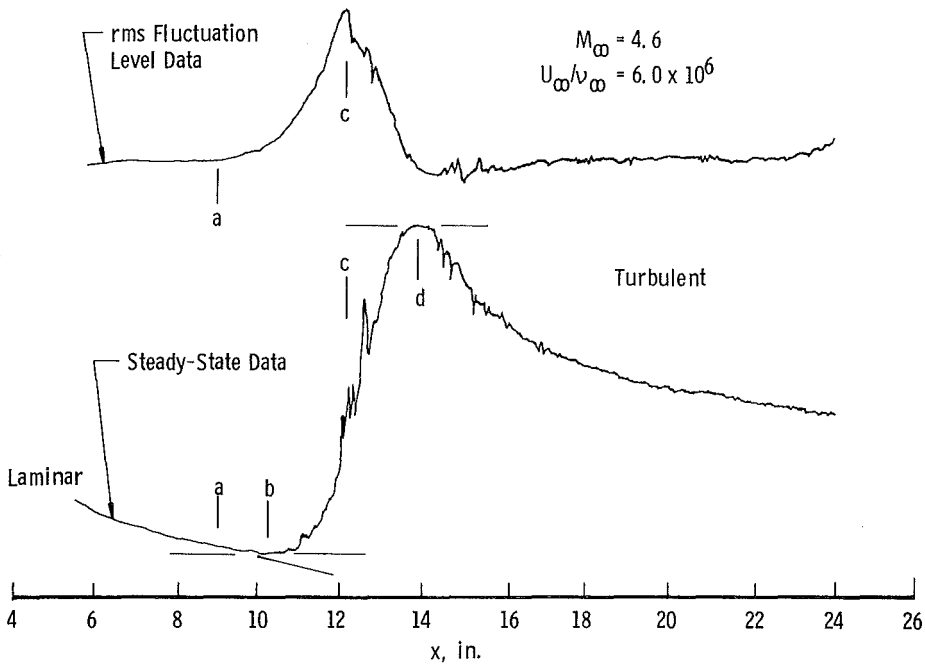

a. High supersonic flow

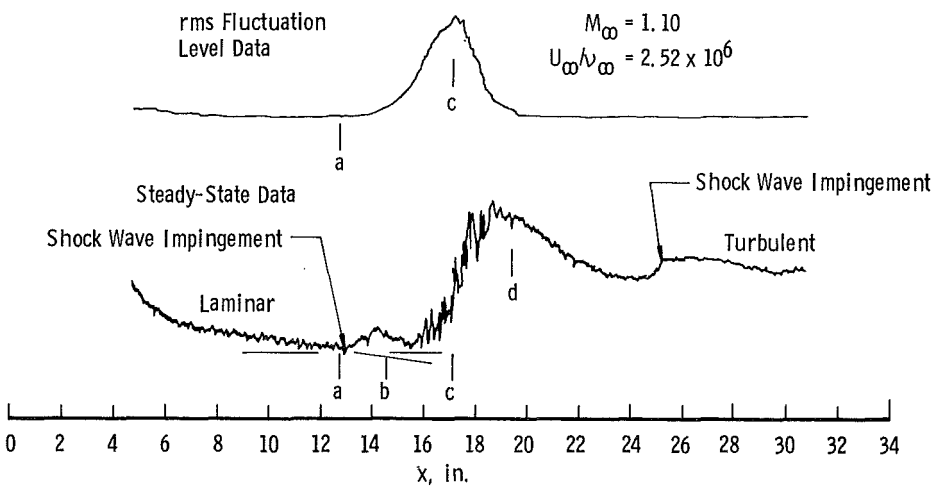

b. Low supersonic flow

Figure 13. Definitions of transition locations in typical pitot probe data traces.

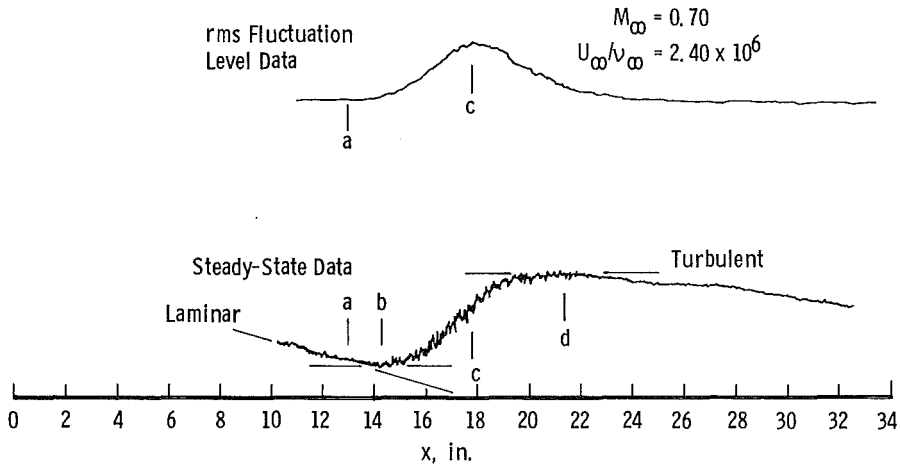

c. Subsonic flow
Figure 13. Concluded.

These four points maintained a nearly constant proportionality in their ratios of lengths from the cone apex at all values of M_∞ and U_∞/ν_∞ so long as the incidence angle was near zero. Among these, point "a" was too poorly defined to be read with any degree of reliability and thus was not used. The points x_t and x_T were selected as primary dependent variables in this investigation; however, the location of the peak steady-state pressure, x_T, was generally much more clearly definable in the majority of the profiles than was the onset of transition, x_t. Accordingly, the end of transition point, x_T, was selected as the primary correlatable variable and x_t was given where possible but with reservations as to its accuracy in definition. Figure 13b also illustrates the difficulty in identification of the transition location at Mach numbers from about 1.05 to 1.3. For these conditions, spurious pressure waves were sometimes sufficiently large to obscure either x_t or x_T. Usually, such perturbations could be associated with a reflection of the bow shock from the test section wall or with some other extraneous source of shock waves in the tunnel.

The movement of the transition zone on the cone surface at M_∞ = 2.0 with varied unit Reynolds number is shown in Fig. 14 to illustrate another facet of these experiments. Lines x_t, x_p, and x_T denoted by open circles, triangles, and squares, are as defined by the pitot probe during a traverse made at each level of U_∞/ν_∞. The closed symbols represent detection of these same three transition points by observing the microphone signals (Fig. 15). While the agreement in x_p is good, the detection of x_t is typically rather poor, being dependent upon precisely how the microphone output was interpreted. The rms level of microphone signal, $\sqrt{p'^2}$, has been normalized by q_∞ to define the fluctuating pressure coefficient, ΔC_p

$$\Delta c_p = \frac{\sqrt{\overline{p}'^2}}{q_\infty} \times 100, \text{ percent} \qquad (1)$$

and is presented in Fig. 15. This agreement indicated that the microphones could be used as a redundant means for detecting the end-of-transition location. Substantiation was also obtained that the transition zone was essentially uniform circumferentially around the cone since the microphone locations were roughly opposite the line of the pitot probe traverse (see Fig. 1).

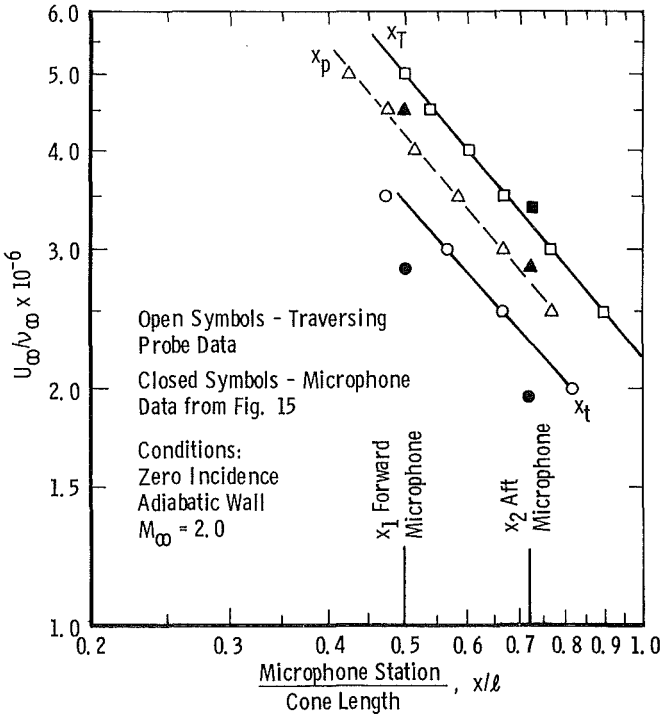

Figure 14. Comparison of transition location between pitot pressure probe and microphone data.

The primary function of the microphones was to indicate the level of free-stream pressure fluctuations imposed on the cone in a given wind tunnel. Furthermore, the maximum peak in fluctuation level in the transition zone was found to be extremely sensitive to the degree of microphone flushness to the wall. Levels of ΔC_p presented in this report are generally those made under laminar conditions.

Repeated observations made by more than one observer, revealed that subjective interpretation of pitot pressure profiles caused an uncertainty in determination of x_T of about ± 0.5 in. (3σ) at the cone midlength ($x/\ell = 0.5$). This corresponds to an

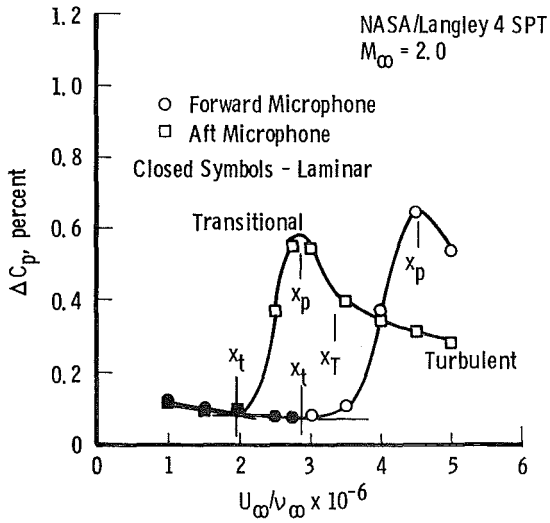

a. Laminar, transitional, turbulent conditions

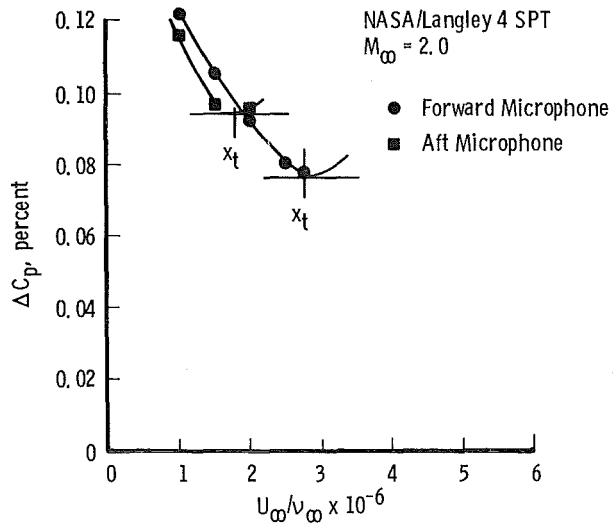

b. Expanded scale of the laminar condition

Figure 15. Typical rms levels measured by microphones as a function of unit Reynolds number.

uncertainty of about ±3 percent in Re_T. The uncertainty in measurements of x_t was worse, since many of the pitot pressure profiles were not as well formed as the previous illustrative examples. Although the point x_p could be defined with better certainty in measurements than could x_t, it was considered the least significant of the three events located by x_t, x_p, and x_T. Only end-of-transition Reynolds numbers, Re_T, are used in

correlations presented in this report; both end and onset of transition Reynolds numbers, Re_T and Re_t, wherever possible, are documented in Volume II for a more detailed presentation of the data.

4.2 TEST PROCEDURE

The basic test procedure was to align the cone (first geometrically, but aerodynamically, if necessary) as carefully as possible to the flow at a given test condition, monitor the cone surface temperature until thermal equilibrium was approached, record the levels of pressure fluctuations and vibrations on the cone microphones and accelerometers, record the levels of various other dynamic sensors that may have been installed for correlation with the cone measurements, and then detect the location of transition by performing a pitot probe traverse. Test section side-wall-mounted microphones were used during the cone tests in many of the tunnels in order to have a correlation of measurements with the cone.

Transition data were acquired at values of U_∞/ν_∞ ranging from as low as 1.0×10^6 to as high as 7.0×10^6 for most of the Mach number range from 0.2 to 5.5 End-of-transition location, x_T, could be detected using the traversing pitot probe from as far aft as 33.5 in. (the aft limit of probe travel) to as far forward as 5.0 in. Onset of transition, x_t, could be detected as far aft as 33.5 in. but only to about 8.0 in. from the apex, because of the relatively smaller laminar boundary-layer thickness.

The basic test procedure was to map as much of the operating envelope as time permitted in terms of the M_∞, U_∞/ν_∞ matrix with a sufficient number of points to define variations in Re_T and ΔC_p at varied U_∞/ν_∞ for constant M_∞, and varied M_∞ for constant U_∞/ν_∞. Except where noted, all data were acquired at zero incidence with the cone structural temperature stabilized.

4.3 DATA REDUCTION

Transition Reynolds numbers were computed directly from the measurements of x_t and x_T. The data were plotted on log-log scales at constant M_∞ in the form of x_T/ℓ and x_t/ℓ versus U_∞/ν_∞. Transition Reynolds numbers for U_∞/ν_∞ levels of 2.0×10^6, 3.0×10^6, and sometimes 4.0×10^6 or more were then computed from a manual fairing of the data on log-log plots. This procedure allowed a direct comparison of results from different tunnels at the same unit Reynolds numbers. Transition Reynolds numbers were also plotted at constant M_∞ as a function of U_∞/ν_∞ on log-log scales. The data were smoothed when possible in the variable density tunnels as a function of M_∞ for constant levels of U_∞/ν_∞ and sometimes as a function of U_∞/ν_∞ for constant M_∞. The data are also tabulated in Volume II in order that the actual measurements be available to the reader in addition to the smoothed curves which are used for correlation in this report.

The overall rms ΔC_p data were likewise cross plotted against M_∞ and U_∞/ν_∞ to provide a presentation of trends in tunnels at the same conditions for which the transition Reynolds number data are presented. Selected pressure fluctuation data, $\overline{p'}$, were subjected to spectral analysis. The choice of Fourier or power density spectral analysis was in part a function of the type of spectra occurring in a given tunnel, e.g., amplitude ratio of certain discrete spectral components to the random broadband spectrum, and in part a function of the particular analysis equipment available at a given facility.

5.0 SUMMARY OF RESULTS

A summary of the measured boundary-layer transition location (defined as the end-of-transition Reynolds number, Re_T) and test section rms noise level (ΔC_p) from the participating wind tunnels listed in Table 2 is given in Volume II. Because of the large volume of data recorded during this investigation, it is impractical to discuss detailed trends observed for each tunnel in this report. However, all of the data for each tunnel are presented in Volume II of this report.

5.1 TRANSITION REYNOLDS NUMBER AND TEST SECTION NOISE LEVEL

Low Noise Level Tunnels (Groups 1, 3, and 4)

A composite of the transition data from most Group 1, 3, and 4 tunnels is shown in Figs. 16a through c. The data show the variation of transition Reynolds number with free-stream Mach number for three levels of free-stream unit Reynolds number. At low Mach numbers ($M_\infty \lesssim 0.5$) Re_T tends to be a constant value lying between 3.5 and 4.0 million. Transition Reynolds number reaches a peak around $M_\infty \approx 1.5$ and exhibits a local minimum somewhere around $M_\infty = 3.5$. Although considerable data scatter exists, an apparent trend of increasing Re_T with increasing U_∞/ν_∞ is evident for Mach numbers greater than unity (Fig. 16d). Below $M_\infty \approx 1.0$, within the data scatter, Re_T is almost independent of U_∞/ν_∞.

A definition of the test section noise level (ΔC_p) for these tunnels is shown in Fig. 17 for $U_\infty/\nu_\infty \approx 3.0$. The noise level was measured during the same test points that transition location measurements were made. The variation of ΔC_p with M_∞ is almost an inverse trend to that of Re_T with M_∞ (see Fig. 16). Although the trends are not an exact inverse, they are near enough so as to suspect that the wind tunnel noise has an influence on transition location in these relatively quiet tunnels. The term noise level used herein loosely encompasses all types of pressure disturbances incident on the cone surface either in the form of acoustic waves or buffeting of the cone laminar boundary layer by turbulence.

High Noise Level Tunnels (Group 2)

Transition Reynolds numbers measured during tests in the perforated-wall transonic tunnels of Group 2 are shown in Fig. 18. These data are presented at the same three levels of U_∞/ν_∞ as shown in Fig. 16 for tunnels of Groups 1, 3, 4, and nonstandard Group 2 cases. As seen in Fig. 18, these data lie in a smaller range of Re_T than the data from the low noise tunnels.

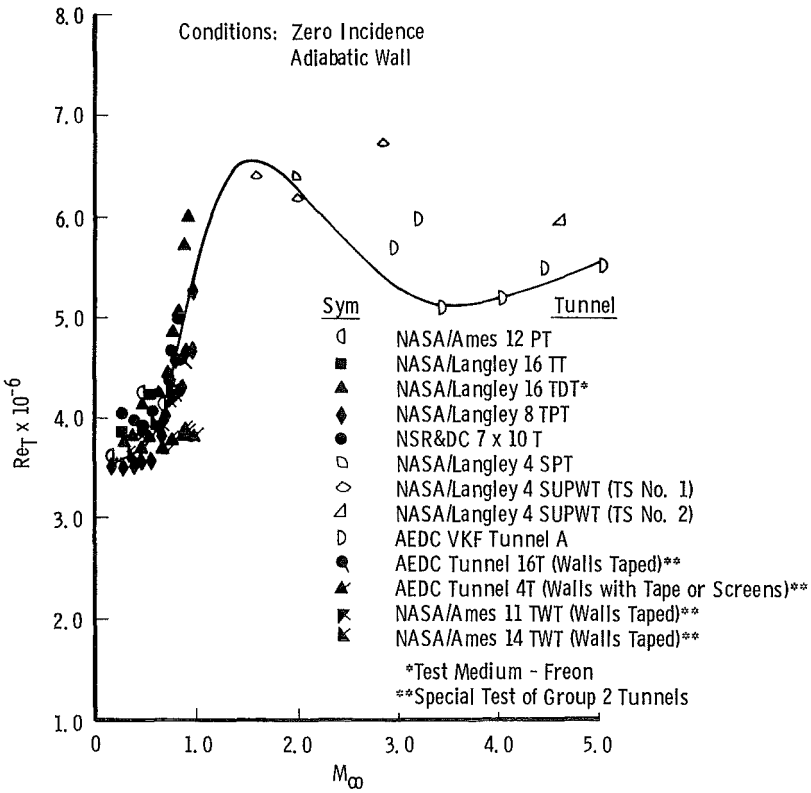

a. $U_\infty/\nu_\infty = 2.0 \times 10^6$

Figure 16. Summary of measured end-of-transition location (Re_T) from Group 1, 3, and 4 tunnels.

Basic noise data (ΔC_p) acquired in Group 2 tunnels are shown in Fig. 19, at a $U_\infty/\nu_\infty \approx 3.0 \times 10^6$; also shown for comparison is a faired curve from the low noise tunnel data of Fig. 17. The lower transition Reynolds numbers in Fig. 18 are seen to be related to higher noise levels in Fig. 19.

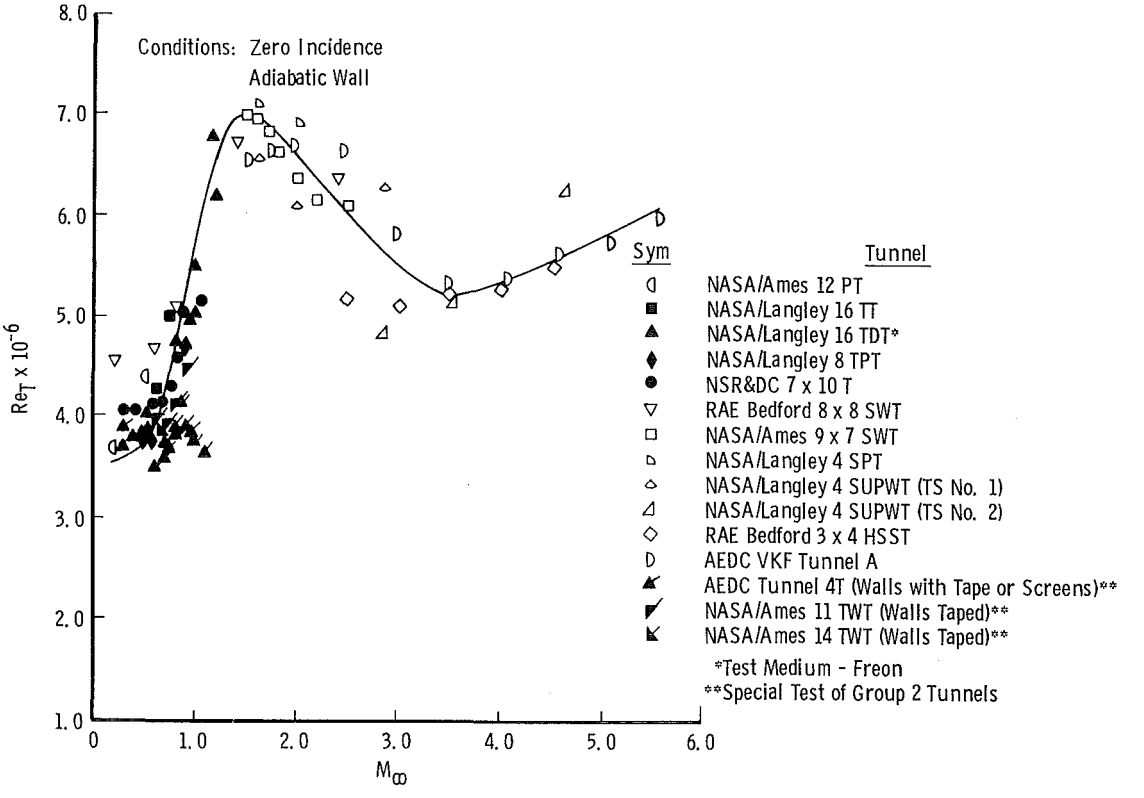

b. $U_\infty/\nu_\infty = 3.0 \times 10^6$

Figure 16. Continued.

A significant reduction in the noise level of these tunnels was effected in four cases by closing the porous walls with tape or covering the porous walls with a fine-mesh screen. The resulting transition and noise characteristics have been shown in Figs. 16 and 17. Further details about this type of noise and the effectiveness of the noise suppression measures are detailed in Ref. 12 and Volume II. The amount of reduction in ΔC_p was as much as a factor of three in these Group 2 tunnels.

Transition Reynolds number is shown as a function of noise level in Fig. 20 for cases where both Re_T and ΔC_p measurements were available at the same test conditions in seventeen of the wind tunnels. The only data which did not appear to fit this simple correlation are those acquired in open-slotted tunnels of Group 1 at certain high subsonic Mach numbers where spectral analysis of the noise data indicated ΔC_p to be dominated by low frequency components (< 200 Hz). The correlation shown in Fig. 20, except for the phantom points, produces a mean trend in Re_T within ± 20 percent of a faired curve given by

$$Re_T = 3.7 \times 10^6 \ (\Delta C_p)^{-1/4} \qquad (2)$$

This correlation gives no consideration to M_∞, U_∞/ν_∞, tunnel size, and tunnel geometry over the range of variables or types of tunnels encompassed in this investigation. Within the limits of data scatter, it appears that Re_T is indeed a function of ΔC_p.

5.2 EFFECTS OF MODEL INCIDENCE AND HEAT TRANSFER

Experiments to determine the influence of incidence angle on transition were performed at U_∞/ν_∞ of nominally 3.0 x 10^6. As shown in Fig. 21, a strong variation in the effect of incidence occurred. The possibility of errors introduced by incidence was greatest on the leeward side at the supersonic Mach numbers. For instance, a 20 percent reduction in Re_T occurs on the leeward ray for an α of only 0.6 deg, at M_∞ = 2.2. However, deviations of less than ±10 percent were noted at all windward angles for $M_\infty \leq$ 2.2. It is doubtful that geometric positioning to aerodynamic stream alignment was routinely as good as ±0.25 deg, because of uncertainties in tunnel flow angularity.

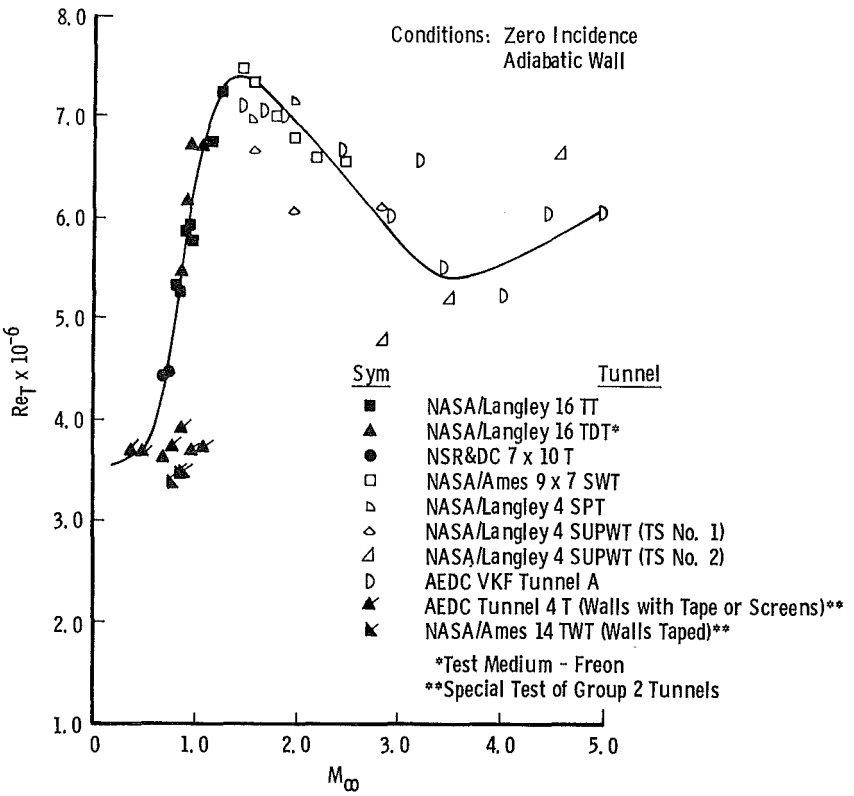

c. U_∞/ν_∞ = 4.0 x 10^6

Figure 16. Continued.

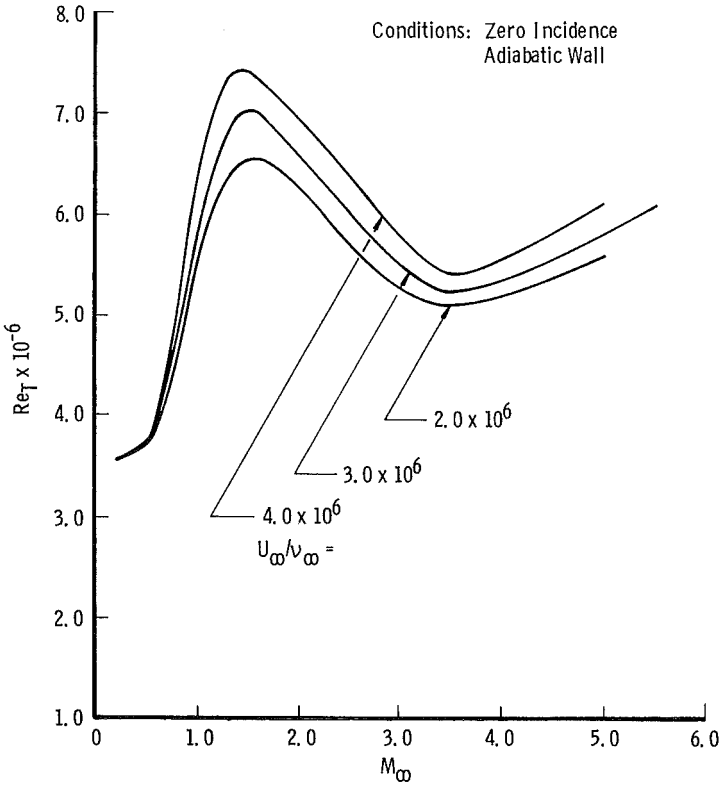

d. Faired trends
Figure 16. Concluded.

The existence of heat transfer between the cone and the free-stream flow can alter the laminar boundary-layer velocity profile and hence its stability characteristics. The present investigation was restricted to only continuous flow wind tunnels where long soak times to achieve thermal equilibrium were possible. (The one exception was the ONERA 2.56 x 1.83 S-3 Modane blowdown wind tunnel where no transition data were acquired.)

Heat transfer was possible when a temperature potential existed during the transient periods of changing flow conditions. The cone surface (T_w) and body (T_B) temperatures (see Fig. 1) were monitored during these transients to assure equality and, hence, thermal equilibrium, before acquiring data.

The experiment performed to gain insight into the influence of heat transfer on transition location was performed in the AEDC Tunnel 4T where it was possible to make rapid changes in total (stagnation) temperature, T_t. At $M_\infty = 1.2$, the cone was allowed to soak for about ten minutes after which T_t was rapidly raised. When T_w had increased to

approximately the adiabatic wall temperature, T_{aw}, T_t was then rapidly lowered. The results are shown in Fig. 22. After the rapid changes in T_t, the cone temperatures, T_w and T_B, lagged behind as shown in Fig. 22a. The rate of convective heat transfer was proportional to the temperature difference (T_{aw}-T_w) shown in Fig. 22b. The effect on transition is indicated in Fig. 22c. Data from transients similarly performed at M_∞ = 0.4

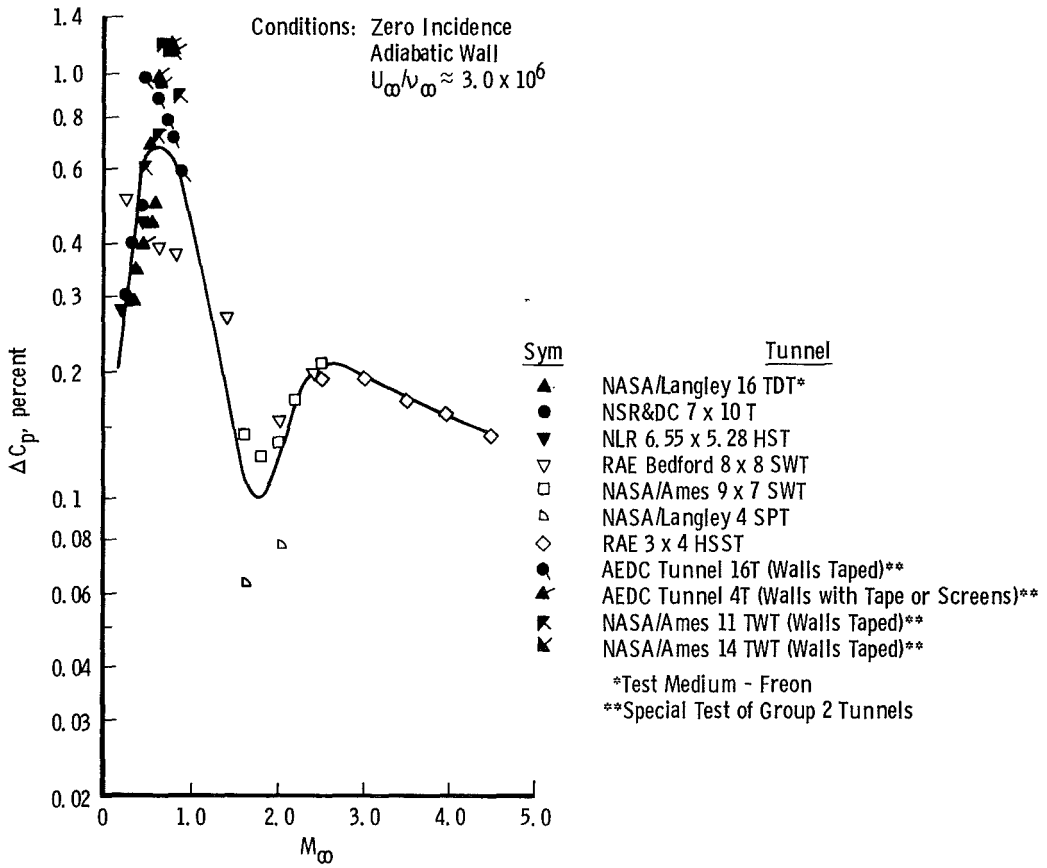

Figure 17. Summary of measured test section rms noise levels (ΔC_p) from Selected Group 1, 3, and 4 tunnels.

are shown in Fig. 23. These data indicate a 10-percent change in transition Reynolds number for only a 10°R change in cone surface temperature (steady-state T_t was nominally 560°R).

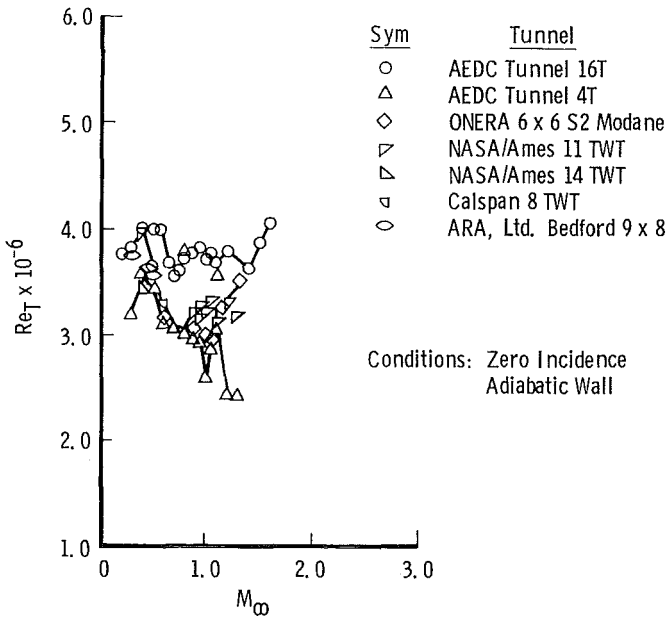

a. $U_\infty/\nu_\infty = 2.0 \times 10^6$

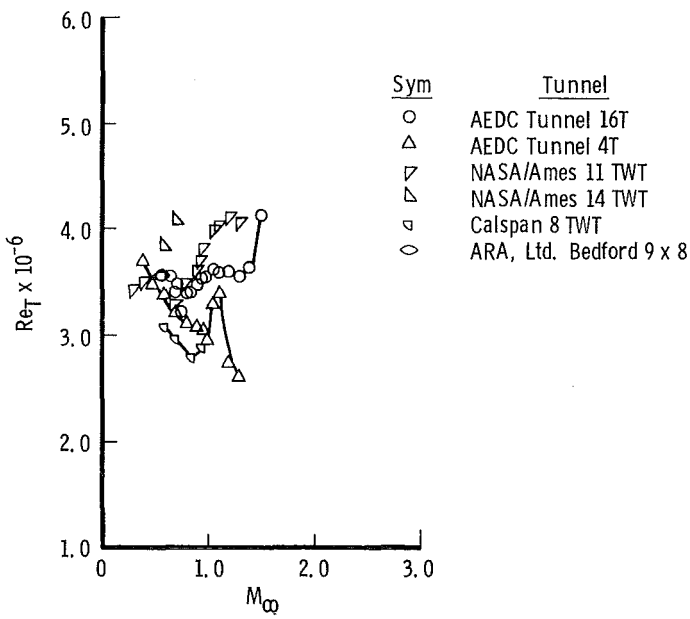

b. $U_\infty/\nu_\infty = 3.0 \times 10^6$

Figure 18. Summary of measured end-of-transition location (Re_T) from Group 2 tunnels.

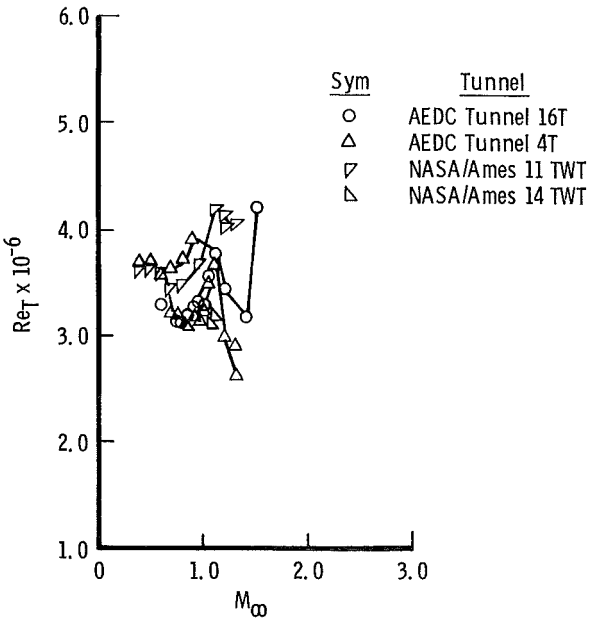

c. $U_\infty/\nu_\infty = 4.0 \times 10^6$

Figure 18. Concluded.

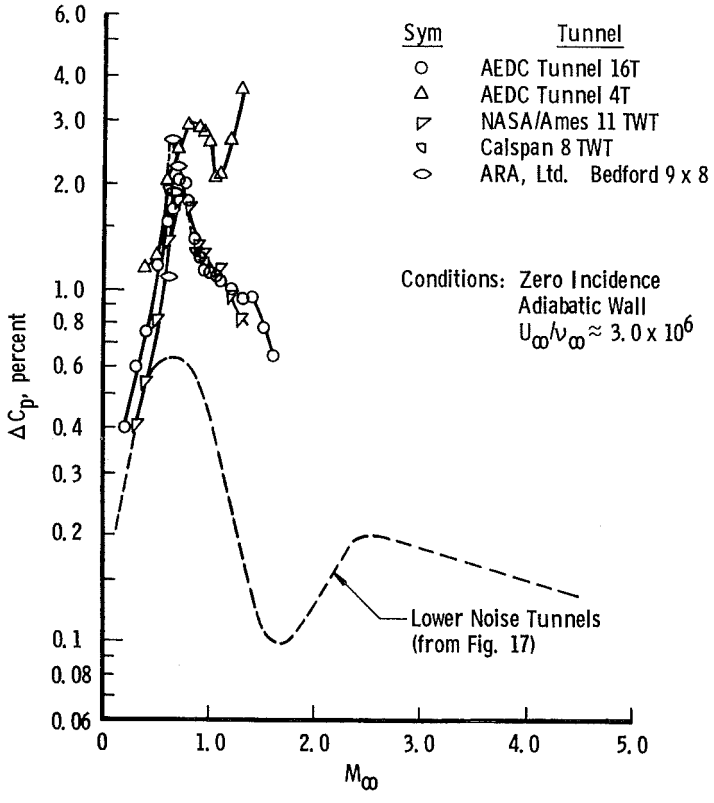

Figure 19. Summary of measured test section rms noise levels (ΔC_p) from selected Group 2 tunnels.

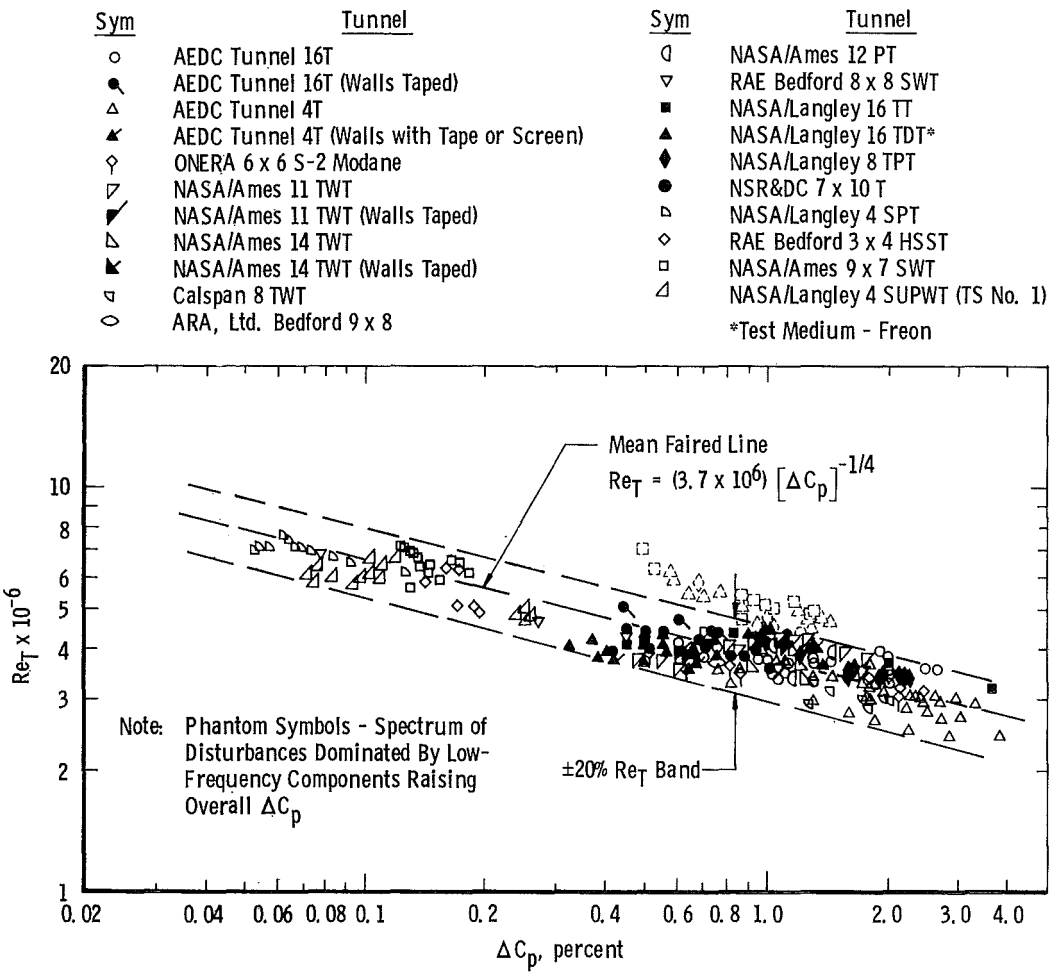

Figure 20. Overall correlation of end-of-transition location (Re_T) with rms noise level (ΔC_p).

Notes:
1. Re_{T_α} Normalized by Re_T at $\alpha = 0$
2. All Data Shown at $\beta = 0$

Sym	M_∞	Tunnel
◕	0.6	NASA/Ames 11 TWT
○	0.95	NASA/Ames 11 TWT
▽	1.3	NASA/Ames 11 TWT
◇	1.6	NASA/Langley 4 SUPWT TS No. 1
□	2.2	NASA/Ames 9 x 7 SWT
◿	4.6	NASA/Langley 4 SUPWT TS No. 2

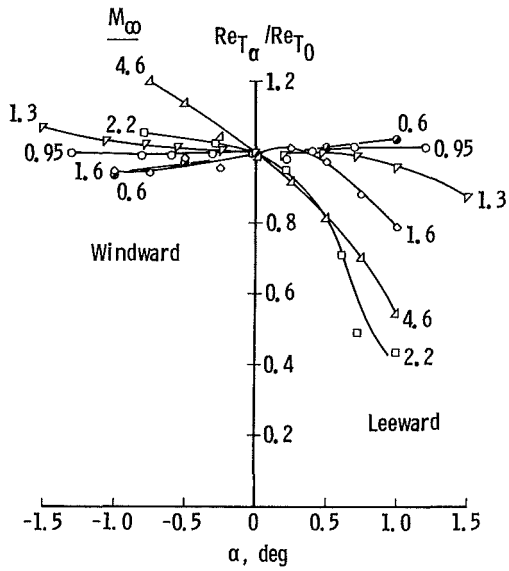

a. Angle-of-attack influence

Notes:
1. Re_{T_β} Normalized by Re_T at $\beta = 0$
2. All Data Shown at $\alpha = 0$

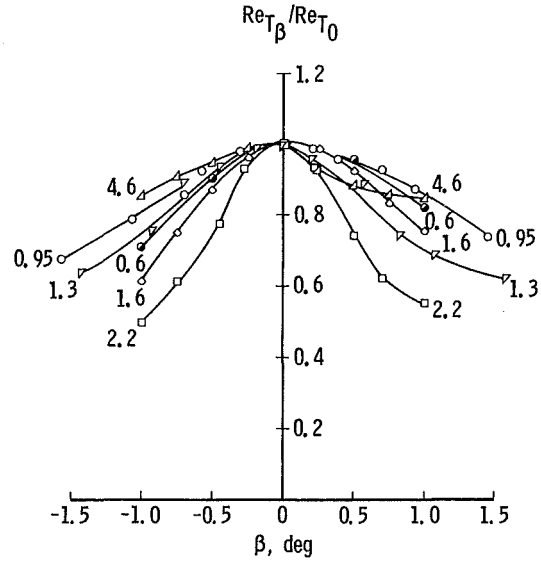

b. Yaw angle influence

Figure 21. Summary of the effect of model incidence angle (α and β) on transition.

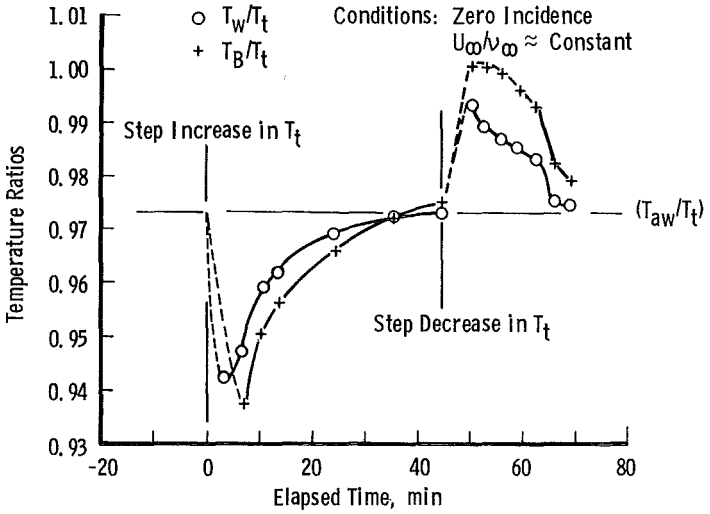

a. History of temperature transients

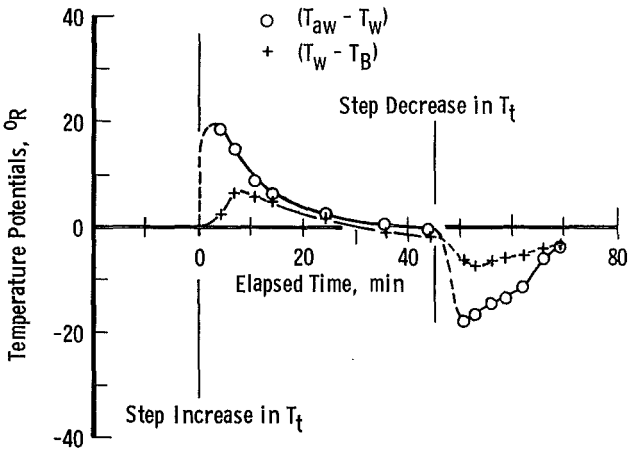

b. History of temperature potentials

Figure 22. Effect of deviations from adiabatic wall temperature on Re_T at M_∞ = 1.20.

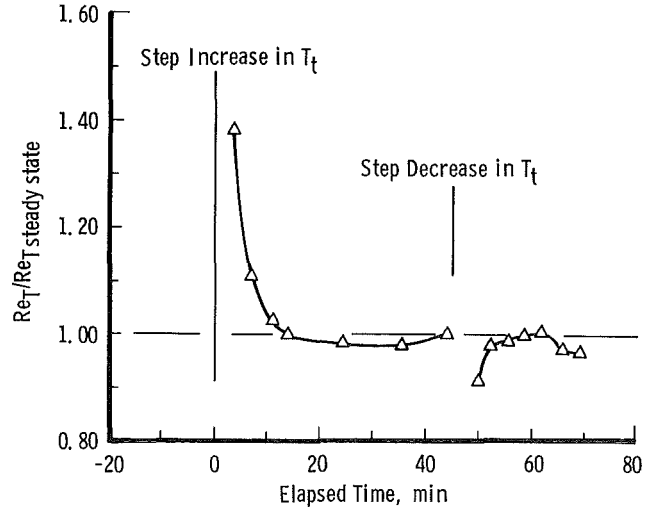

c. Movement in transition location
Figure 22. Concluded.

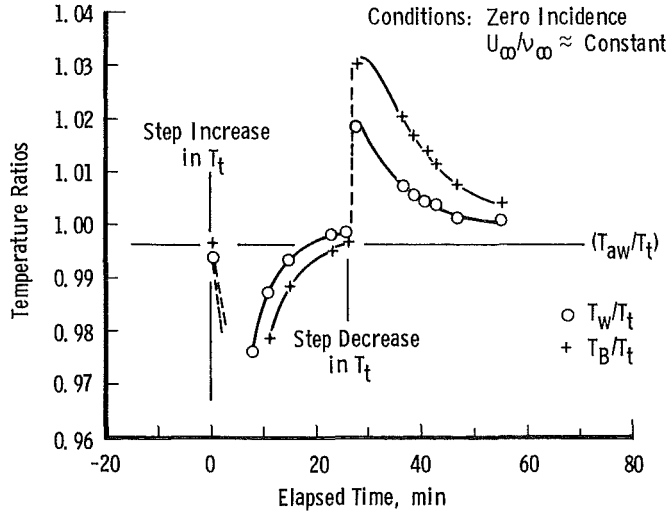

a. History of temperature transients
Figure 23. Effect of deviations from adiabatic wall temperature on Re_T at $M_\infty = 0.4$.

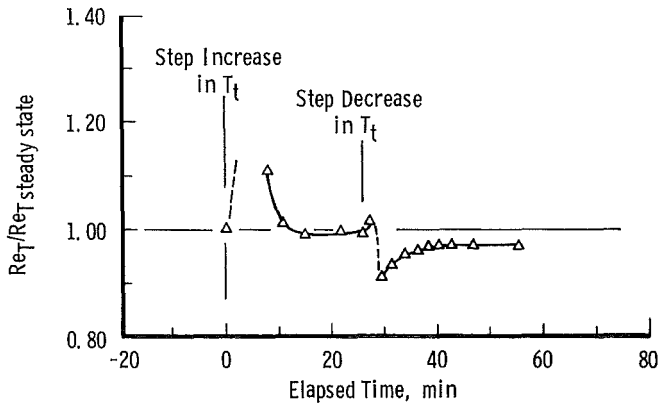

b. Movement in transition location
Figure 23. Concluded.

6.0 CONCLUDING REMARKS

An extensive experimental investigation was carried out in 23 wind tunnels, in several countries, to document effects of wind tunnel test section noise level on boundary-layer transition location on a 10-deg included-angle cone. Care was taken to maintain the cone in the same physical condition for each experiment and to make measurements using the same techniques each time. Additional precautions were taken to eliminate the unwanted influence of model incidence and heat transfer on the transition measurements. A summary of the data is compiled in Volume I and complete sets of data from all tunnels are given in Volume II.

Analysis of the data, obtained over the Mach number range from 0.2 to 5.5, indicated definable trends in transition Reynolds number with Mach number and unit Reynolds number. These trends were explainable within about ±20 percent by trends in the test section noise level. Controlled changes constituting reduction of noise levels in some wind tunnels produced corresponding increases in transition Reynolds number. Practically all values of transition Reynolds number were correlated when scaled to the inverse 1/4 power of the overall root-mean-square noise level. Care should be exercised in extending these results directly to other configurations.

REFERENCES

1. Potter, J. L. and Whitfield, J. D. "Preliminary Study of the Effect of Unit Reynolds Number on Transition Sensitive Data." AEDC-TN-57-37 (AD135338), September 1957.

2. Whitfield, J. D. and Potter, J. L. "The Unit Reynolds Number as a Parameter in Boundary Layer Stability." AEDC-TN-58-77 (AD202731), October 1958.

3. Potter, J. L., Whitfield, J. D., and Strike, W. T. "Transition Measurements and the Correlation of Transition Sensitive Data." AEDC-TR-59-4 (AD208775), February 1959.

4. Potter, J. L. and Whitfield, J. D. "Effects of Slight Nose Bluntness and Roughness on Boundary-Layer Transition in Supersonic Flows." Journal of Fluid Mechanics, Vol. 12, No. 4, 1962, pp. 501-535.

5. Potter, J. L. and Whitfield, J. D. "Boundary-Layer Transition Under Hypersonic Conditions." AEDC-TR-65-99 (AD462716), May 1965; Presented at the AGARD Specialists' Meeting on "Recent Developments in Boundary Layer Research." Naples, Italy, AGARDograph 97, Part III, May 1965.

6. Pate, S. R. and Schueler, C. J. "Effects of Radiated Aerodynamic Noise on Model Boundary-Layer Transition in Supersonic and Hypersonic Wind Tunnels." AEDC-TR-67-236 (AD666644), March 1968.

7. Pate, S. R. "Measurements and Correlations of Transition Reynolds Numbers on Sharp Slender Cones at High Speeds." AEDC-TR-69-172 (AD698326), December 1969.

8. Pate, S. R. and Brown, M. D. "Acoustic Measurements in Supersonic Transitional Boundary Layers." AEDC-TR-69-182 (AD694071), October 1969.

9. Credle, O. P. and Carleton, W. E. "Determination of Transition Reynolds Number in the Transonic Mach Number Range." AEDC-TR-70-218 (AD275995), October 1970.

10. Dougherty, N. S., Jr. and Steinle, F. W., Jr. "Transition Reynolds Number Comparisons in Several Major Transonic Tunnels." AIAA Paper No. 74-627, Presented at the AIAA 8th Aerodynamic Testing Conference, Bethesda, Maryland, July 8-10, 1974.

11. Anonymous. "Instructions and Applications, One-Quarter Inch Condenser Microphones Type 4135/4136." Bruel and Kjaer Manual, July 1971.

12. Dougherty, N. S., Jr. "A Study of Acoustic Disturbances and Means of Suppression in Ventilated Transonic Wind Tunnel Walls." AEDC-TR-77-67 (ADA045347), October 1977.

NOMENCLATURE

a_∞	Free-stream speed of sound
ΔC_p	rms pressure fluctuations normalized with q_∞ and expressed in percent, $\sqrt{\overline{p'^2}}/q_\infty$
f	Frequency, cycles/sec or Hz
ℓ	Cone surface length (36 in. without extension)
M_∞	Free-stream Mach number, U_∞/a_∞
p_∞	Free-stream static pressure
$\overline{p}'$	Fluctuating static pressure
p_t	Tunnel total pressure
q_∞	Free-stream dynamic pressure, $(1/2)\rho_\infty U_\infty^2$
Re_T	Transition Reynolds number based on x_T
Re_t	Transition Reynolds number based on x_t
rms	Root-means-square, e.g., of fluctuating static pressure, $\sqrt{\overline{p'^2}}$
T_∞	Free-stream static temperature
T_B	Cone body temperature
T_t	Tunnel total temperature
T_w	Cone surface temperature
T_{aw}	Adiabatic wall recovery temperature
t	Time, min
U_∞	Free-stream velocity computed from M_∞ and T_∞, ft/sec
U_∞/ν_∞	Free-stream unit Reynolds number, 1/ft
x	Surface distance from cone apex

x_p, x_T, x_t — Surface distance to measured transition defined in Section 4.1

α — Cone model angle of attack, deg

β — Cone model angle of yaw, deg

μ_∞ — Dynamic viscosity

ν_∞ — Kinematic viscosity, μ_∞/ρ_∞

ρ — Free-stream density

θ_c — Cone half-angle, deg

SUBSCRIPTS

aw — Adiabatic wall, cone surface

B — Cone body (interior bore surface)

p — Location of peak in fluctuations during transition

∞ — Free-stream conditions

T — End-of-transition location

t — Onset of transition location, also total conditions

w — Cone wall (surface)

α — At angle of attack

β — At angle of yaw

0 — At zero incidence

1 — Forward microphone location, 18 in.

2 — Aft microphone location, 26 in.